https://doi.org/10.1093/brain/awad016 BRAIN 2023: 146; 2828–2845 | 2828

BRAIN
ORIGINAL ARTICLE

The Interictal Suppression Hypothesis in focal epilepsy: network-level supporting evidence

Graham W. Johnson,[1,2,3] Derek J. Doss,[1,2,3] Victoria L. Morgan,[1,2,3,4,5,6] Danika L. Paulo,[4] Leon Y. Cai,[1,2,3] Jared S. Shless,[2,3,4] Aarushi S. Negi,[7] Abhijeet Gummadavelli,[4] Hakmook Kang,[8] Shilpa B. Reddy,[9] Robert P. Naftel,[4] Sarah K. Bick,[4] Shawniqua Williams Roberson,[5] Benoit M. Dawant,[1,2,3,4,6,10] Mark T. Wallace[11,12,13,14] and Dario J. Englot[1,2,3,4,6,10]

Why are people with focal epilepsy not continuously having seizures? Previous neuronal signalling work has implicated gamma-aminobutyric acid balance as integral to seizure generation and termination, but is a high-level distributed brain network involved in suppressing seizures? Recent intracranial electrographic evidence has suggested that seizure-onset zones have increased inward connectivity that could be associated with interictal suppression of seizure activity. Accordingly, we hypothesize that seizure-onset zones are actively suppressed by the rest of the brain network during interictal states.

Full testing of this hypothesis would require collaboration across multiple domains of neuroscience. We focused on partially testing this hypothesis at the electrographic network level within 81 individuals with drug-resistant focal epilepsy undergoing presurgical evaluation. We used intracranial electrographic resting-state and neurostimulation recordings to evaluate the network connectivity of seizure onset, early propagation and non-involved zones. We then used diffusion imaging to acquire estimates of white-matter connectivity to evaluate structure–function coupling effects on connectivity findings. Finally, we generated a resting-state classification model to assist clinicians in detecting seizure-onset and propagation zones without the need for multiple ictal recordings.

Our findings indicate that seizure onset and early propagation zones demonstrate markedly increased inwards connectivity and decreased outwards connectivity using both resting-state (one-way ANOVA, P-value $= 3.13 \times 10^{-13}$) and neurostimulation analyses to evaluate evoked responses (one-way ANOVA, P-value $= 2.5 \times 10^{-3}$). When controlling for the distance between regions, the difference between inwards and outwards connectivity remained stable up to 80 mm between brain connections (two-way repeated measures ANOVA, group effect P-value of 2.6×10^{-12}). Structure–function coupling analyses revealed that seizure-onset zones exhibit abnormally enhanced coupling (hypercoupling) of surrounding regions compared to presumably healthy tissue (two-way repeated measures ANOVA, interaction effect P-value of 9.76×10^{-21}). Using these observations, our support vector classification models achieved a maximum held-out testing set accuracy of $92.0 \pm 2.2\%$ to classify early propagation and seizure-onset zones.

These results suggest that seizure-onset zones are actively segregated and suppressed by a widespread brain network. Furthermore, this electrographically observed functional suppression is disproportionate to any observed structural connectivity alterations of the seizure-onset zones. These findings have implications for the identification of seizure-onset zones using only brief electrographic recordings to reduce patient morbidity and augment the presurgical evaluation of drug-resistant epilepsy. Further testing of the interictal suppression hypothesis can provide insight into potential new resective, ablative and neuromodulation approaches to improve surgical success rates in those suffering from drug-resistant focal epilepsy.

Received August 01, 2022. Revised December 24, 2022. Accepted January 08, 2023. Advance access publication February 1, 2023
© The Author(s) 2023. Published by Oxford University Press on behalf of the Guarantors of Brain. All rights reserved. For permissions, please e-mail: journals.permissions@oup.com

1 Department of Biomedical Engineering, Vanderbilt University, Nashville, TN 37235, USA
2 Vanderbilt University Institute of Imaging Science (VUIIS), Vanderbilt University Medical Center, Nashville, TN 37232, USA
3 Vanderbilt Institute for Surgery and Engineering (VISE), Vanderbilt University, Nashville, TN 37235, USA
4 Department of Neurological Surgery, Vanderbilt University Medical Center, Nashville, TN 37232, USA
5 Department of Neurology, Vanderbilt University Medical Center, Nashville, TN 37232, USA
6 Department of Radiological Sciences, Vanderbilt University Medical Center, Nashville, TN 37232, USA
7 Department of Neuroscience, Vanderbilt University, Nashville, TN 37232, USA
8 Department of Biostatistics, Vanderbilt University, Nashville, TN 37232, USA
9 Department of Pediatrics, Vanderbilt Children's Hospital, Nashville, TN 37232, USA
10 Department of Electrical Engineering and Computer Science, Vanderbilt University, Nashville, TN 37235, USA
11 Department of Hearing and Speech Sciences, Vanderbilt University, Nashville, TN 37232, USA
12 Department of Psychology, Vanderbilt University, Nashville, TN 37232, USA
13 Department of Psychiatry and Behavioral Sciences, Vanderbilt University, Nashville, TN 37232, USA
14 Department of Pharmacology, Vanderbilt University, Nashville, TN 37232, USA

Correspondence to: Graham W. Johnson
Vanderbilt University, 1500 21st Avenue South
VAV 4340, Nashville, TN 37212, USA
E-mail: grahamwjohnson@gmail.com

Keywords: epilepsy; connectivity; inhibition excitation; EEG; diffusion imaging

Introduction

Drug-resistant focal epilepsy (DRE) accounts for 30–40% of the estimated 50 million cases of epilepsy worldwide.[1,2] If medication fails to control seizures, patients may elect to pursue surgical treatments including resection,[3,4] ablation[5,6] or neurostimulation.[7,8] Traditional presurgical evaluation includes identification of seizure-onset zones (SOZs) using seizure semiology, non-invasive neuroimaging and scalp EEG.[9] SOZs are defined as observed sites of ictal onset and are candidates for an electro-clinically defined 'epileptogenic zone' that could theoretically be removed to render the patient seizure free.[10] If these techniques fail to accurately localize SOZs, then invasive monitoring with stereotactic-EEG (SEEG) can be pursued.[11] To properly localize SOZs with SEEG, the patient must remain in the hospital for days to weeks to record many seizures (ictal events).[12,13] To reduce the morbidity of long intracranial recordings, brief resting-state (interictal) SEEG analysis has shown promise in identifying SOZs.[14–20]

Resting-state SEEG studies often use the conceptual framework of epilepsy as a disorder of interconnected brain nodes (i.e. a network).[21–26] Specifically, recent work has shown that SOZs exhibit increased inwards interictal connectivity from other nodes of the brain.[20,27] This work has led us to propose the Interictal Suppression Hypothesis (ISH), which posits that the SOZ is tonically suppressed by other areas of the brain during the resting state to prevent seizure initiation (Fig. 1). The premise of this hypothesis is intuitively based on the clinical observation that people with DRE are not continuously having seizures, so perhaps there is an interictal, widespread functional organization of the brain that is actively suppressing epileptiform activity. Further, neurophysiological evidence for this hypothesis has been demonstrated in animal models showing GABA (γ-aminobutyric acid) -mediated receptor tonic interictal inhibition of SOZs.[28,29] A complete testing of the ISH requires collaboration across many domains of neuroscience, including molecular, cellular and brain network investigations using both animal models and human data. In humans, specifically, we can partially test the ISH by using SEEG electrodes to investigate the connectivity of the epileptic network. SEEG signal observations are electrical phenomena of underlying physiological activity that provide direct sampling of brain tissue, offering insight into the high-level functional organization of the brain in humans with DRE.

Beyond resting-state recordings, SEEG electrodes can also be used to electrically stimulate the brain. Specifically, single-pulse electrical stimulation (SPES) can be used to simultaneously stimulate one region and record the poststimulation EEG signal (evoked response) at all other implanted regions.[30–34] SPES provides another paradigm to test the ISH. Importantly, not only can directionality be inferred from SPES, but relative elevation or attenuation of oscillatory activity can also be quantified to gain insight into the relative excitatory and inhibitory nature of functional connections. Specifically, a power spectral density (PSD) approach[34–36] can build on previous works that focused on whole-band power metrics, such as root mean square,[37–39] or metrics that rely on cortico-cortical evoked potential waveform morphology that can be difficult to interpret with depth electrodes due to the inconsistency of evoked potential amplitude due to orientation uncertainty relative to pyramidal neurons.[30,40–44] The interpretation of SOZ spectral response to SPES can offer insight into the seizure-onset network beyond the capabilities of resting-state functional connectivity analyses because it can quantify elevation or attenuation of neural activity by measuring the change in oscillatory activity in response to perturbing a distant brain node.

Finally, the spatial and anatomical characteristics of the network (i.e. structural connectivity) have been shown to affect the resting-state and stimulation-derived network characteristics. Specifically, past work has suggested that short-range connections drive increased SOZ connectivity,[19] and diffusion-weighted imaging (DWI) derived structural connectivity helps explain the network's functional connections.[40,45] Thus, we will evaluate resting-state connectivity as it relates to SEEG contact spacing across the brain. Furthermore, we will use DWI to capture more

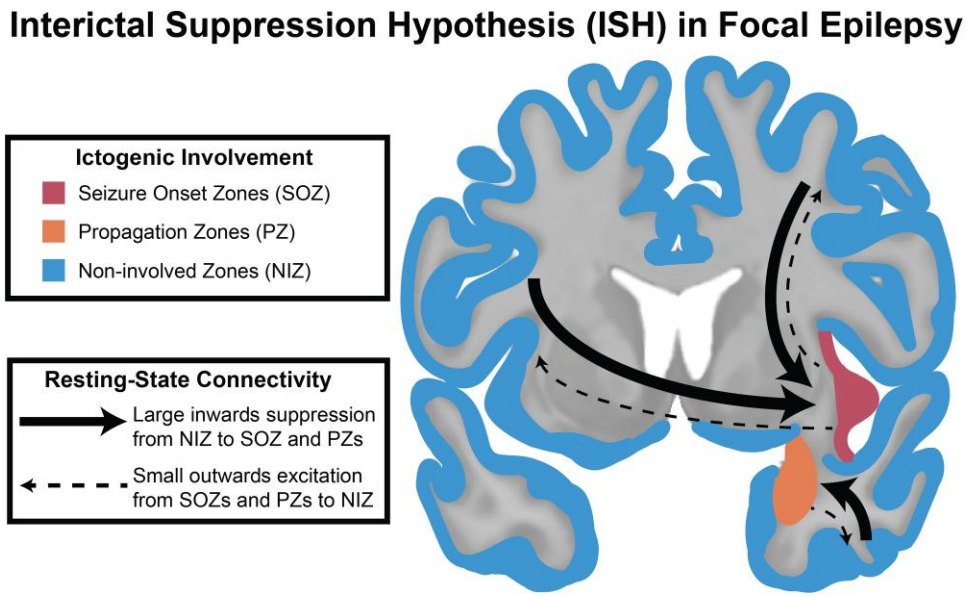

Figure 1 ISH in focal epilepsy. The ISH proposes that regions not involved in ictogenesis (NIZ, blue) have an active role in suppressing SOZ and early PZ through brain network interactions that can be observed electrographically.

specific structural connectivity information between SEEG contacts. Past work that addresses the nuisance effect of structural connectivity as it relates to functional connectivity has been limited by reduction of the SEEG sampling space to atlas parcellations or relies on biased seeding techniques that do not generalize well across a patient cohort with diverse SEEG implantation schemes. A more sophisticated technique is probably required to capture the structural connectivity that each individual SEEG contact is sampling. Thus, we use a new contact-specific structural connectivity paradigm that is not biased by SEEG implantation scheme. Using these techniques, we can evaluate the effects of distance and structural connectivity to draw conclusions about any pathological changes to structure–function coupling of the seizure-onset network.

Overall, this work aims to partially test the ISH at the brain network level using resting-state and stimulation-based electrophysiology, controlling for spatial and anatomical variability using DWI. This work cannot provide complete testing of the ISH and is simply an investigation that uses some of the most direct techniques currently available to explore human brain networks. Better characterization of SOZs using only interictal data may reduce patient morbidity by reducing reliance on ictal recordings and provide insight into the underlying biophysical pathophysiology of the epileptic network.

Materials and methods

To interrogate the ISH electrographically and structurally, we performed a series of analyses with resting-state SEEG, SPES and DWI to evaluate the high-level brain network organization in focal epilepsy. The results of these analyses were tested against multiple null hypotheses that include: (i) organization of the seizure-onset network exhibits indistinguishable resting-state connectivity to that of regions outside the seizure-onset network; (ii) edge distance does not correlate with SOZ/PZ/NIZ directed network connectivity; (iii) SOZ and PZs respond identically to NIZs when the SEEG implanted network is stimulated; and (iv) differences in functional connectivity are proportionally coupled to underlying differences in structural connectivity.

Participants and seizure network designations

We included 81 patients with DRE undergoing SEEG presurgical evaluation at Vanderbilt University Medical Center (VUMC). Important demographic and clinical variables are outlined in Table 1. This study was approved by Vanderbilt's Institutional Review Board and all patients provided informed consent. The diagnosis of DRE and decision to pursue SEEG were determined by VUMC's standard multidisciplinary process, including epileptologists, neurosurgeons and neuropsychologists. This process included analysis of patient history, seizure semiology, video EEG, MRI, PET, memory/language localization by functional MRI or Wada, and neuropsychological testing. Electrode (Ad-Tech or PMT Cooperation) trajectories were planned by treating physicians according to standard clinical care at VUMC using the CRAnial Vault Explorer (CRAVE; Vanderbilt University, Nashville, TN, USA).[46] Each patient had an average of 124.3 ± 31.4 [mean $\pm$ standard deviation (SD)] SEEG contacts implanted.

To assign seizure network designations to the SEEG contacts, the treating epileptologist reviewed all electroclinical ictal events during the SEEG monitoring. SOZs were defined as SEEG contact(s) with the first electrographic epileptiform changes observed for a clinically significant ictal event. Early propagation zones (PZs) were defined as SEEG contacts with electrographic epileptiform activity spread within 10 s of ictal onset on the basis of previous work outlining clinical relevance of identifying areas of seizure spread.[47] Non-involved zone (NIZ) SEEG contacts were defined as belonging to neither SOZ nor PZ designations.[19,20] The review was blinded to clinically presumed epilepsy subtype, any surgical treatment and surgical outcome. Next, a single expert reviewed all epileptologist designations of SOZ/PZ/NIZ. Finally, to quantify response to surgical intervention we calculated the Engel Surgical

Table 1 Subject demographics and clinical information

	Full cohort ($n = 81$)	SPES subcohort ($n = 23$)	Diffusion subcohort ($n = 26$)
Sex, female (n, %)	46 (56.8%)	16 (69.6%)	20 (76.9%)
Age (years, mean ± SD)	34.4 ± 12.1	36.7 ± 11.7	35.2 ± 11.5
Epilepsy duration (years, mean ± SD)	16.4 ± 11.9	15.1 ± 9.0	14.8 ± 10.6
FBTC seizures, yes (n, %)	58 (71.6%)	18 (78.2%)	17 (65.4%)
MTS, yes (n, %)	15 (18.5%)	3 (13.0%)	6 (23.1%)
Clinically presumed epilepsy subtype (n, %)			
Unilateral mTLE	28 (34.6%)	8 (34.8%)	12 (46.2%)
Bilateral mTLE	12 (14.8%)	3 (13.0%)	4 (15.4%)
Unilateral lateral TLE	10 (12.3%)	4 (17.4%)	2 (7.7%)
Unilateral frontal lobe epilepsy	11 (13.6%)	2 (8.7%)	1 (3.8%)
Unilateral parietal lobe epilepsy	4 (4.9%)	1 (4.3%)	2 (7.7%)
Multiple presumed foci (not bilateral mTLE)	16 (19.8%)	5 (21.7%)	5 (19.2%)
Surgery type (n, %)			
Resective SAH	14 (17.3%)	3 (13.0%)	8 (30.8%)
ATL	11 (13.6%)	3 (13.0%)	3 (11.5%)
Other resection	10 (12.3%)	1 (4.3%)	2 (7.7%)
Laser SAH	4 (4.9%)	0 (0%)	0 (0%)
RNS	24 (29.6%)	10 (43.5%)	11 (42.3%)
DBS	1 (1.2%)	0 (0%)	0 (0%)
None	17 (21.0%)	6 (26.1%)	2 (7.7%)
Follow-up duration[a] (months, mean ± SD)	26.7 ± 17.6	12.8 ± 7.8	35.3 ± 19.0
SEEG nodes implanted (n, mean ± SD)	124.3 ± 31.4	133.5 ± 23.6	127.5 ± 23.9
SEEG nodes in grey matter (n, mean ± SD)	85.4 ± 26.7	93.3 ± 19.0	78.8 ± 23.9
SEEG nodes stimulated (n, mean ± SD)	NA	60.0 ± 10.7	NA
SEEG node designations (n, mean ± SD)			
SOZ	11.2 ± 9.2	13.7 ± 11.2	12.2 ± 9.6
PZ	9.0 ± 10.3	7.6 ± 7.4	6.24 ± 6.9
NIZ	65.2 ± 23.4	72.0 ± 18.6	66.9 ± 21.6

ATL = anterior temporal lobectomy; DBS = deep brain stimulation of bilateral anterior thalamic nuclei; FBTC = focal to bilateral tonic-clonic seizures; mTLE = mesial temporal lobe epilepsy; MTS = mesial temporal sclerosis; RNS = responsive neurostimulation; SAH = selective amygdalohippocampectomy; TLE = temporal lobe epilepsy.
[a]Only for resective surgeries.

Outcome Scale for subjects who received a resective or ablative surgery and had follow-up data at least 1 year following surgery.[48] Patients who received a neuromodulation treatment were excluded from surgical outcome analyses.

Resting-state stereotactic-EEG connectivity

We calculated undirected and directed SEEG resting-state connectivity for all 81 subjects as outlined in our previous studies.[19,20] Briefly, we collected 20 min of resting-state data on SEEG post-implantation Day 1 or 2, with the subject lying flat with their eyes closed trying not to fall asleep. We then filtered the data with a 1–59, 61–119, 121–150 Hz bandpass Butterworth filter using MATLAB'S filtfilt function (MathWorks Inc., Natick, MA, USA) to remove direct current offset and power line interference. The signals were referenced using a bipolar montage. For simplicity, each bipolar pair referenced signal will henceforth be referred to as a 'node' and the connectivity between two nodes will be referred to as an 'edge'. To reduce potential segmentation bias, we did not use a brain atlas for any portion of these analyses.[49] Avoiding potentially arbitrary region segmentations increases the generalizability of these analytical approaches and improves biological interpretation by only accounting for tissue that is directly sampled by SEEG. We then segmented the 20-min resting-state epoch into ten 2-min epochs. All metric calculations described next were averaged across these ten 2-min epochs.

To assess undirected resting-state SEEG connectivity, we calculated imaginary coherence (ImCoh) and real coherence for all edges.[19] ImCoh ignores zero-time lag signals and reduces volume conduction and artefact effects.[50,51] Specifically, alpha-band ImCoh has the highest test–retest reliability and has been well established as a measure of functional connectivity,[52,53] including in intracranial EEG studies.[51] For directed connectivity analysis, we calculated partial directed coherence (PDC) for all edges.[20] A node's undirected connectivity was defined as the average ImCoh value of that node's edges with respect to all other nodes (i.e. 'strength' of the node). A node's outwards connectivity was defined as the average outwards PDC of edges with respect to all other nodes. Correspondingly, a node's inwards connectivity was defined as the average inwards PDC of edges from all other nodes. To quantify the overall direction of a node's connectivity, reciprocal connectivity was calculated as the difference between each node's inwards and outwards connectivity. Reciprocal connectivity is directly correlated to the inwards/outwards connectivity but simplifies analyses to a single metric that attempts to capture the balance between incoming and outgoing node connections. In all circumstances, intra-patient normalization with z-scoring was done for each connectivity matrix (i.e. whole-matrix mean subtracted and divided by whole-matrix standard deviation) to homogenize the dynamic range of connectivity values. All connectivity was analysed in the theta (4–7 Hz), alpha (8–12 Hz), beta (12–30 Hz), low-gamma (31–80 Hz) and high-gamma (81–150 Hz) oscillatory bands. To test our results against the null hypothesis that SOZs and PZs exhibit similar connectivity to that of NIZs, we used a one-way ANOVA as our omnibus test with *post hoc*

Tukey–Kramer multiple comparison corrections. Additionally, we investigated whether mesial temporal lobe epilepsy (mTLE) and non-mTLE exhibited differences in SOZ/PZ/NIZ connectivity—we split the full cohort into mTLE ($c = 40$) and non-mTLE ($n = 41$) and ran a two-way ANOVA with *post hoc* one-way ANOVAs for each group separately.

Futhermore, to evaluate the effect of distance on connectivity measurements, we calculated the Euclidean distance between all nodes (centroid of the bipolar pair) using CRAVE software. We then re-calculated all functional connectivity measurements with Euclidean edge distance thresholds of 5–20, 20–35, 35–50, 50–65 and 65–80 mm. These distance thresholds were chosen to include a roughly equal number of SEEG nodes across a wide range of Euclidean distances for the entire subject cohort. In this manner, we were able to observe the effect of distance between the SEEG nodes on the functional connectivity measurements. To test against the null hypothesis that distance does not correlate with connectivity and that SOZs and PZs exhibit similar connectivity to NIZs, we used a two-way repeated measure ANOVA.

Finally, owing to the PDC normalization scheme, there is potential mathematical bias introduced into the analyses because each patient has a different number of SEEG channels. Furthermore, there are fewer SOZ and PZ designations per patient compared to NIZ that could affect the final statistics. Last, for the distance analyses, the local connections outnumber the long connections and could bias the results. To address these concerns, we conducted the following bootstrapping approaches with 250 complete re-calculations of PDC for each iteration: (i) resting-state PDC with only 5, 10 or 20 random channels from each category of SOZ, PZ and NIZ for each patient, and with 40 out of 81 random patients selected for each iteration; and (ii) distance analysis PDC with only 10, 50 or 100 random edges (i.e. connections between SEEG channels) selected for each distance bin for each patient, and with 40 out of 81 random patients selected for each iteration. These highly conservative bootstrapping approaches can test the stability of the results and address concerns about imbalance in the raw datasets.

Single-pulse electrical stimulation connectivity

To further test the ISH, we collected neurostimulation data from the most recently enrolled subset of 23 patients in the cohort. Specifically, we conducted SPES with every SEEG node in grey matter for each patient, resulting in 60.0 ± 10.7 (mean ± SD) nodes stimulated per patient. We used 10-second trains of 1 Hz, 300 µs, biphasic pulses at 3.0 mA with a recording sampling rate of 512 Hz. We filtered raw SEEG data using MATLAB'S filtfilt function with Butterworth filters with passbands of 1–59, 61–119 and 121–151 Hz. We then parsed the data into epochs of 5–305 ms following each stimulation pulse. This poststimulation epoch has been previously outlined to capture most SPES-induced electrographic changes.[31] The initial 5 ms epoch following stimulation and all nodes within 20 mm of stimulation were omitted to avoid stimulation artefacts.[54]

We then created SPES-derived connectivity matrices by computing the PSD for the frequency bands outlined in the section 'Resting-state SEEG connectivity'. The PSD for each node was normalized to that node's prestimulation baseline value. The outwards connectivity for a given node was assigned as the PSD change from baseline within a given frequency range for all non-stimulated SEEG nodes when that node was stimulated. Conversely, the inwards connectivity for a given node was assigned as the PSD change from the prestimulation baseline in the frequency band of interest for that node when all other nodes had been stimulated separately. All PSD measurements were averaged across the 10 redundant stimulation pulses to increase the signal-to-noise ratio. We did not attempt to analyse any frequencies below 4 Hz due to the short sampling window poststimulation. To test our results against the null hypothesis that SOZs and PZs show similar stimulation-derived connectivity to that of NIZ, we used a one-way analysis of variance (ANOVA) as our omnibus test with *post hoc* multiple comparisons with Tukey–Kramer corrections. Additionally, we investigated whether mTLE and non-mTLE SOZ/PZs responded differently to SPES using a two-way ANOVA.

Diffusion imaging collection and preprocessing

We collected DWI data using high angular resolution diffusion imaging acquisition with 92 *b*-vector directions at a *b*-value of 1600 s/mm^2. We preprocessed the DWI data with the PreQual pipeline built around MRTrix3,[55] FSL[56] and ANTs[57] software packages.[58] First, the diffusion data were denoised with the Marchenko–Pastur PCA method.[59–61] The images were then intensity-normalized to the first image and concatenated for further processing. No reverse phase encoded images were acquired, but corresponding T_1 images of the subjects were available. Thus, a T_1 image was used to generate a synthetic susceptibility-corrected b0 volume using SYNB0-DISCO, a deep learning framework by Schilling *et al.*[62] This synthetic b0 image was used in conjunction with FSL's topup to correct for susceptibility-induced artefacts in the diffusion data. FSL's eddy algorithm was then used to correct motion artefacts and eddy currents and to remove outlier slices.[63–66]

Patient-specific stereotactic-EEG-based structural connectivity: the SWiNDL technique

Next, we sought to evaluate the structure–function coupling between brain regions sampled by SEEG. To accurately quantify the structural connectivity between SEEG electrodes, we implemented a novel technique termed 'subsampling whole-brain tractography with iEEG near-field dynamic localization' (SWiNDL). We developed this technique to obtain a patent-specific SEEG contact-to-contact structural connectome by using the group analysis advantages of anatomically constrained whole-brain tractography and spherical-deconvolution filtering of tractograms (SIFT2).[67]

First, we performed whole-brain tractography using MRtrix3 with SIFT2 weighting to generate 10 million streamlines.[55,67] Briefly this included brain extraction from the T_1 image,[68] bias field correction[69] and registration to DWI.[70] The T_1 image was then be used to create five-tissue type[71–73] segmentations. Spherical deconvolution was performed on the preprocessed DWI to get direct fibre orientation density function for every voxel.[74,75] We then performed probabilistic tractography[76] using the five-tissue type volume to perform anatomically constrained tractography[77] with dynamic seeding.[46] The resulting tractogram was then corrected using SIFT2 for improved biological accuracy of white-matter representation.[67,78]

We next localized each patient's SEEG electrodes using CRAVE. We assigned a three-dimensional Gaussian probability distribution around each SEEG contact to model the volume of tissue electrically sampled by that electrode—we used a 95% attenuation of the probability at 12 mm based off previous electrophysiological work characterizing the spatial dynamics of local field potentials.[79] For the connection between each pair of SEEG contacts (i.e. an edge), we

then took the raw tractogram of 10 million streamlines and assigned dynamic weights [0–1] to each streamline based on the location of the endpoints relative to the SEEG contacts. For example, a streamline would be highly sampled by the SWiNDL algorithm with a weight close to 1.0 if each endpoint were near the centre of a contact. Whereas, if one or both endpoints were far from the two SEEG contacts of interest, then that streamline would be assigned a weight close to 0.0 based off the minimum Gaussian distribution value of the two contacts. The weighted sum of the 10 million streamlines for each bivariate pair of contacts is summed to achieve the structural connectivity for that edge. SWiNDL allows for patient-specific SEEG contact-level connectomes that are dynamically weighted to the proximity of streamlines to the contacts and does not rely on inconsistent probabilistic tractography seeding between patients.

Using the SWiNDL structural connectivity, we calculated the average connectivity for SOZs, PZs and NIZs across a subset of 26 subjects that had available diffusion imaging. Finally, we evaluated the structure–function coupling by calculating the ratio of structural to functional connectivity for each SEEG edge in a patient. Specifically, we divided the intra-patient raw SWiNDL structural connectivity (all positive values) by the raw functional connectivity (all positive values), followed by intra-patient *z*-scoring. Thus, large negative values of this coupling measure indicate a very low relative value of structural connectivity divided by functional connectivity. Thus, we termed any connections that had disproportionality high functional connectivity compared to average or low structural connectivity as 'hypercoupled'. To test against the null hypothesis that distance does not correlate with structure–function coupling, and that SOZs and PZs exhibit similar coupling to NIZs, we used a two-way repeated measure ANOVA.

Stereotactic-EEG node classification model

Using the functional and structural connectivity metrics outlined before, we sought to test the efficacy of a support vector machine (SVM) classification of individual SEEG nodes (i.e. bipolar channel pairs) as SOZ, PZ or NIZ. For all SVM model development and evaluation, we used a 5-fold nested cross-validation scheme that uses a completely held-out test set for each fold of model training and validation. In this way, we can repeatedly test a model's generalizability while minimizing overfitting the training data. All fold splits were conducted at the patient level. We implemented a weighted loss function to account for class imbalance.

First, we developed a model to classify each SEEG node as SOZ, PZ or NIZ using only the resting-state functional connectivity metrics of ImCoh and PDC (6928 SEEG nodes for 81 subjects). Next, we sought to evaluate whether the model improved with the addition of patient-specific structural connectivity metrics obtained from SWiNDL evaluation of DWI (2051 SEEG nodes from 26 subjects). Finally, we trained a model using only functional data from subjects who received resective or ablative therapy and achieved Engel I (free of disabling seizures) outcomes at least 1 year after surgery (1431 SEEG nodes from 19 subjects), and then evaluated the model on subjects who received resective or ablative therapy with Engel II–IV (not seizure free) surgical outcomes (1265 SEEG nodes from 15 subjects).

Data availability

Data may be made available upon reasonable request.

Results

Seizure-onset zones and propagation zones exhibit evidence of network suppression at rest

Resting-state SEEG analysis with 81 subjects revealed that SOZs and PZs exhibit significantly increased undirected connectivity compared to NIZs. These undirected results were consistent across all frequency bands for ImCoh, apart from high gamma (one-way ANOVA P-value < 0.05 for delta to low-gamma bands; Supplementary Fig. 1). The real coherence results demonstrated similar significance to ImCoh across all frequency bands with the exception of high gamma—i.e. real coherence showed a significant difference in the high-gamma band (one-way ANOVA P-value = 4.89×10^{-3}; Supplementary Fig. 2), whereas ImCoh calculations demonstrated no difference across SOZ/PZ/NIZ for the high-gamma band (one-way ANOVA P-value = 7.05×10^{-1}). The alpha-band ImCoh results are depicted in Fig. 2A (one-way ANOVA, P-value = 2.13×10^{-3} with *post hoc* multiple pairwise *t*-test comparisons depicted in the figure).

For the directed analysis, SOZs and PZs demonstrated markedly elevated inwards connectivity and lower outwards connectivity compared to NIZs. More specifically, the mean PZ inwards and outwards connectivity was significantly different from that of SOZs and NIZs (Fig. 2B and C; one-way ANOVA, $P = 1.75 \times 10^{-12}$ and 4.95×10^{-10} for inwards and outwards respectively, with *post hoc* *t*-test $P < 0.05$ for all comparisons). The reciprocal connectivity (inwards–outwards) exhibited an increased significance with a one-way ANOVA P-value of 3.13×10^{-13} (Fig. 2D). The directed connectivity results were consistent across all frequency bands (one-way ANOVA, $P < 1 \times 10^{-10}$ for reciprocal connectivity over all bands, Supplemental Figs 3–5). When analysing mTLE versus non-mTLE, two-way ANOVA 'group' variables (statistic for mTLE versus non-mTLE) ranged from $P = 5.77 \times 10^{-3}$ to 3.91×10^{-2} across all six frequency bands. Whereas, SOZ/PZ/NIZ differences remained strong across the cohort with P-values ranging from 1.49×10^{-15} to 7.06×10^{-13} across bands. These results indicate a slightly significant difference between mTLE and non-MTLE. However, *post hoc* one-way ANOVAs exhibited P-values ranging from $P = 6.22 \times 10^{-11}$ to 1.32×10^{-8} for mTLE and $P = 7.00 \times 10^{-6}$ to 1.49×10^{-4} for non-mTLE. This demonstrates that increased inwards and decreased outwards connectivity of SOZs is observed for both mTLE and non-mTLE, with mTLE showing a larger effect size. The bootstrapping analyses revealed stability of observed differences in SOZ connectivity down to a very conservative subsampling of five random channels per SOZ/PZ/NIZ designation and 40 random patients per iteration (Supplementary Figs 6–11). The results across all metrics and all frequency bands are summarized in Supplementary Table 1. Overall, these findings suggest that high-level functional organization of the epileptic network, as observed on resting-state SEEG, shows a very high inwards flow of information to SOZs and PZs characterized by elevated inwards connectivity and lower outwards connectivity.

Low-frequency power attenuated and high-frequency power augmented in SOZs when network stimulated

When conducting SPES on non-SOZ SEEG contacts, we observed that the SOZ power was markedly attenuated compared to baseline and significantly attenuated compared to NIZs in the lowest frequency band measured (theta, 4–7 Hz) for the 23 patients consented for stimulation (Fig. 3A; SOZ single-population *t*-test, $P = 2.28 \times 10^{-4}$, one-way ANOVA, $P = 2.50 \times 10^{-3}$, *post hoc* pairwise *t*-test comparison

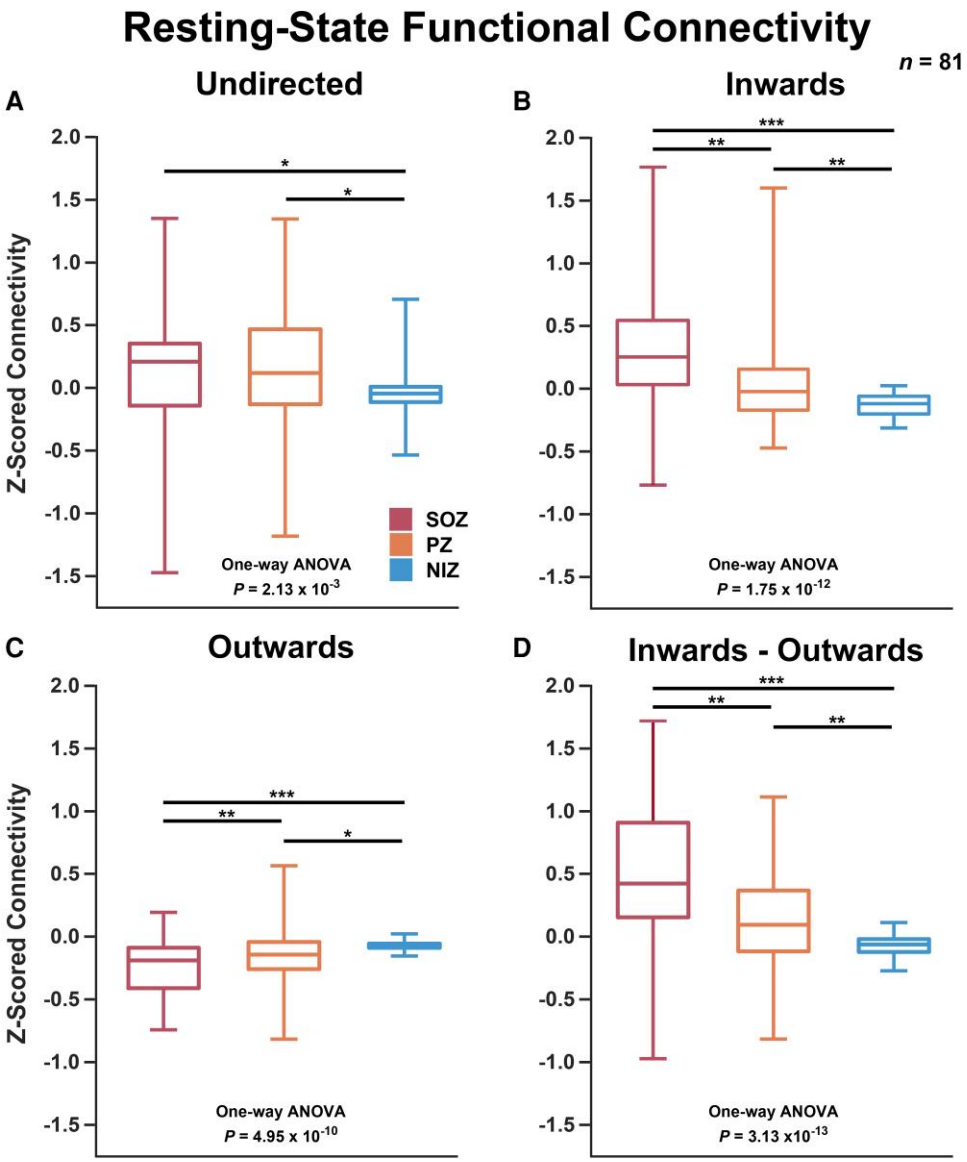

Figure 2 Resting-state SEEG connectivity. (**A**) Undirected alpha-band ImCoh was elevated for SOZs and PZs (one-way ANOVA $P = 2.13 \times 10^{-3}$ with *post hoc* multiple pairwise *t*-test comparisons significant for SOZ-NIZ and PZ-NIZ. (**B**) Inwards PDC strength was elevated significantly for SOZs and PZs (one-way ANOVA $P = 1.75 \times 10^{-12}$ with *post hoc* multiple pairwise *t*-test comparisons significant between all three groups. (**C**) Outwards PDC strength was significantly lower for SOZs and PZs (one-way ANOVA $P = 4.95 \times 10^{-10}$ with *post hoc* multiple pairwise *t*-test comparisons significant between all three groups. (**D**) Inwards—outwards (reciprocal) connectivity exhibited a stronger signal to that of inwards or outwards separately (one-way ANOVA $P = 3.13 \times 10^{-13}$ with *post hoc* multiple pairwise *t*-test comparisons significant between all three groups). Box represents first quartile, mean and third quartile. Whiskers represent maximum and minimum. $^{*}P < 5 \times 10^{-2}$, $^{**}P < 5 \times 10^{-3}$, $^{***}P < 5 \times 10^{-6}$. $n = 81$ subjects.

SOZ-NIZ, $P = 1.80 \times 10^{-3}$). The SOZ and PZ power was not significantly altered in the alpha band (8–12 Hz) (Fig. 3B). The SOZ and PZ power was elevated compared to baseline in beta (13–30 Hz), low-gamma (31–80 Hz) and high-gamma (81–150 Hz) bands, but *post hoc* multiple comparisons revealed that the SOZ elevation in power was only significantly different from NIZs in the beta band and only from PZs in the low and high-gamma bands (Fig. 3C–E; beta: SOZ single-population *t*-test $P = 9.00 \times 10^{-3}$, one-way ANOVA $P = 2.98 \times 10^{-2}$, *post hoc* pairwise *t*-test comparison SOZ-NIZ $P = 2.24 \times 10^{-2}$; low gamma: SOZ single-population *t*-test $P = 6.70 \times 10^{-3}$, one-way ANOVA $P = 1.11 \times 10^{-2}$, *post hoc* pairwise *t*-test comparison SOZ-PZ $P = 1.33 \times 10^{-2}$, high gamma: SOZ single-population *t*-test $P = 7.5 \times 10^{-3}$, one-way ANOVA $P = 3.72 \times 10^{-2}$, *post hoc* pairwise *t*-test comparison SOZ-PZ $P = 2.83 \times 10^{-2}$). When analysing the results across frequency bands for each SOZ, PZ and NIZ separately, both SOZs and NIZs demonstrated a significantly different response to SPES across frequency bands (one-way ANOVA $P = 2.02 \times 10^{-5}$ for SOZ and $P = 0.02$ for NIZ; Fig. 3F). There was no observed statistically significant difference in mTLE versus non-mTLE response to SPES as tested with a two-way ANOVA (Supplementary Fig. 12). These results indicate that low-frequency power is markedly attenuated and high-frequency power is elevated in SOZs when other nodes of the network are stimulated.

Inwards versus outwards connectivity remains constant over long distances

When evaluating the effects of distance on functional connectivity on all 81 patients in the cohort, we observed that both

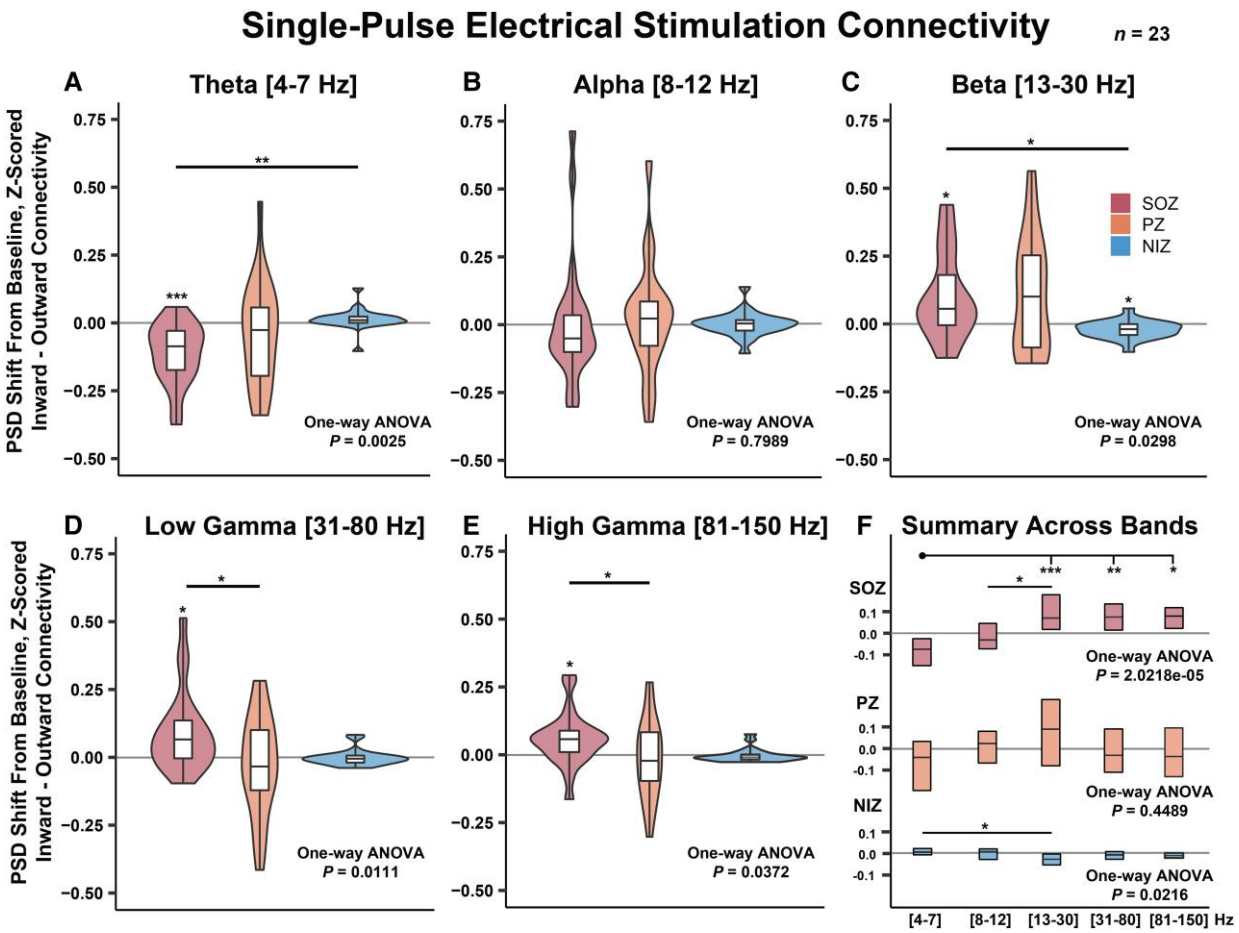

Figure 3 SPES connectivity. Frequency-band specific low-frequency stimulation-induced change in PSD from prestimulation baseline. (**A**) SOZ theta power is reduced when non-SOZ SEEG contacts are stimulated. (**B**) Alpha-band power was not observed to be significantly altered during stimulation. (**C**–**E**) Beta, low-gamma and high-gamma band power in SOZs were elevated when non-SOZs were stimulated. (**F**) The inner quartiles are shown from plots **A**–**E** and separate one-way ANOVAs were conducted for each SOZ, PZ and NIZ separately. $^{*}P < 5 \times 10^{-2}$, $^{**}P < 5 \times 10^{-3}$, $^{***}P < 5 \times 10^{-6}$. $n = 23$ subjects.

undirected and directed connectivity dropped significantly as Euclidean edge length increased (Fig. 4A–C; two-way repeated measures ANOVA distance effect $P < 1 \times 10^{-10}$ for undirected inwards and outwards connectivity). Furthermore, the SOZ, PZ and NIZ undirected connectivity 95% confidence intervals of the mean overlapped significantly for edge distances >20 mm. However, inwards and outwards connectivity for SOZs, PZs and NIZs remained significantly different from each other over the span of Euclidean edge distances (two-way repeated measures ANOVA group effect $P < 1 \times 10^{-10}$ for inwards and outwards). Calculating the reciprocal connectivity over distance, we observed that the relationship between inwards versus outwards connectivity remained mostly consistent over the span of distances as can be observed by the flattening of the trends in Fig. 4D compared to prior plots (two-way repeated measures ANOVA group effect $P = 2.6 \times 10^{-12}$, interaction $P = 1.15 \times 10^{-6}$). The bootstrapping analyses revealed stability of these results down to a very conservative subsampling of 50 random edges per distance bin and 40 random patients per iteration (Supplementary Figs 13–18). The average Euclidean edge distance for intra-SOZ edges, intra-PZ edges and intra-NIZ edges is summarized in Supplementary Table 2. Overall, these results indicate that the network's potential functional suppression of SOZs and PZs, as measured by increased inwards connectivity and decreased outwards connectivity, scales proportionally as distance increases—thus suggesting whole network involvement in SOZ and PZ activity regulation despite the apparent large contribution of only local regions.

Seizure onset zones exhibit local structure–function hypercoupling

Using the SWiNDL technique on 26 patients with DWI available, we observed that SOZs and PZs demonstrated comparably increased structural connectivity compared to NIZs despite only SOZs exhibiting significantly increased reciprocal functional connectivity in this cohort (Fig. 5A; structural: one-way ANOVA $P = 5.18 \times 10^{-7}$, SOZ-PZ $P = 1.2 \times 10^{-3}$, SOZ-NIZ $P = 3.30 \times 10^{-7}$; functional: one-way ANOVA $P = 2.92 \times 10^{-8}$, SOZ-NIZ $P = 7.88 \times 10^{-7}$, PZ-NIZ $P = 5.13 \times 10^{-7}$). This suggests that SOZs have enhanced functional connectivity over PZs despite a comparable SEEG-specific structural connectivity.

We then observed that only the local (5–20 mm) structural connectivity of SOZ and PZs appears to be driving the observed increase in structural connectivity over NIZs due to the overlapping of 95% confidence intervals for all distance thresholds >20 mm (Fig. 5B). However, the structure–function hypercoupling of SOZs was significantly stronger extending to 35 mm

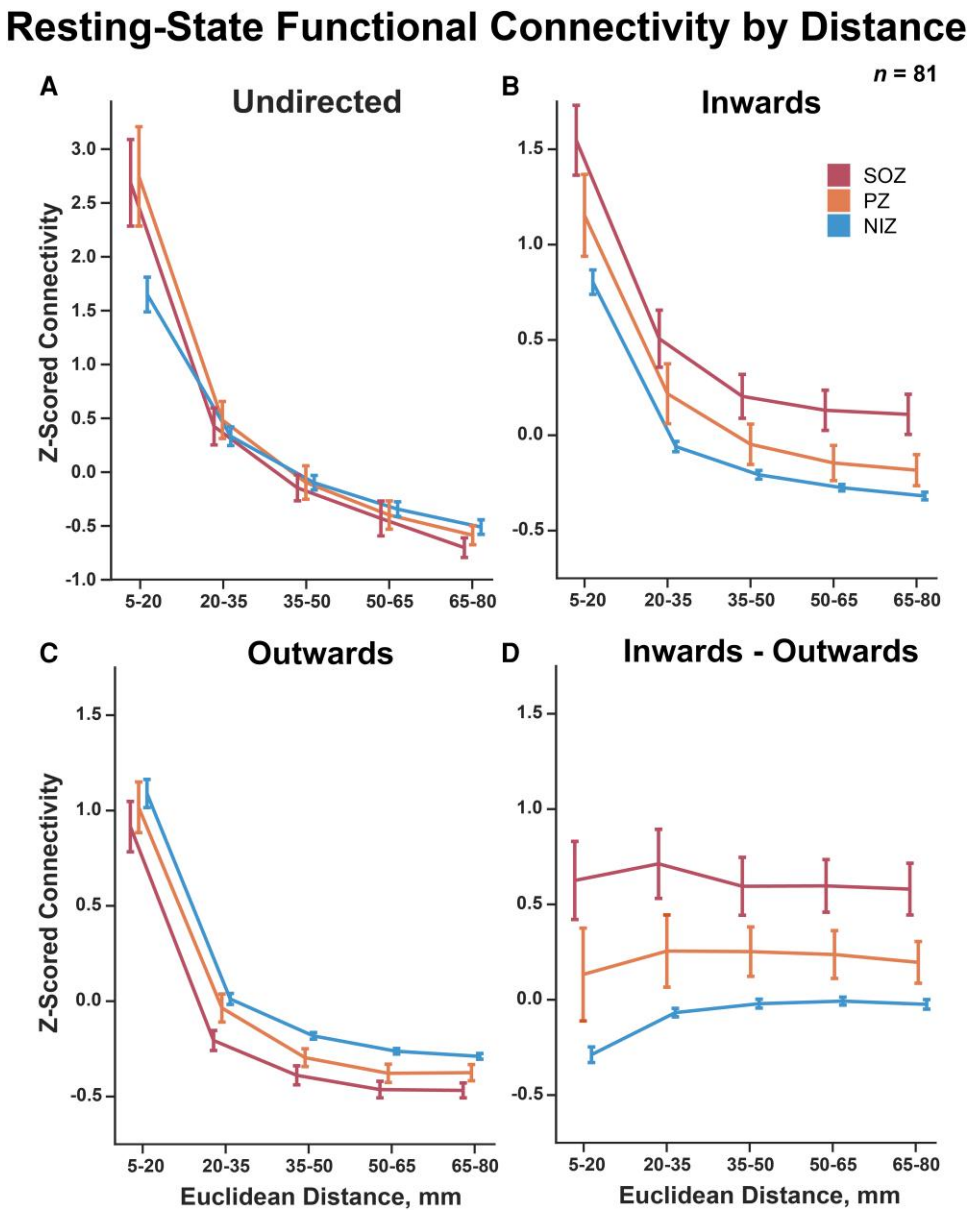

Figure 4 SEEG resting-state connectivity over Euclidean distance. (**A–C**) Undirected and directed connectivity declined rapidly with increasing network edge Euclidean distance thresholds (two-way repeated measures ANOVA distance effect P-value $< 1 \times 10^{-10}$ for undirected inwards and outwards connectivity). (**D**) Reciprocal connectivity (inwards–outwards PDC strength) demonstrates a consistent relationship spanning all distance thresholds measured (two-way repeated measures ANOVA group effect P-value $= 2.6 \times 10^{-12}$, interaction P-value $= 1.15 \times 10^{-6}$). Error bars represent 95% confidence intervals of the mean.

compared to NIZs, with PZs exhibiting an intermediate local (5–20 mm) structure–function hypercoupling (Fig. 5C; two-way repeated measures ANOVA group effect $P = 7.27 \times 10^{-4}$, distance effect $P = 8.63 \times 10^{-19}$, interaction $P = 9.76 \times 10^{-21}$). These results indicate that SOZs exhibit an inherently increased resting-state structure–function hypercoupling over short to medium range distances despite a comparable structural connectivity to that of PZs.

Propagation zone connectivity differs based on surgical outcome

When re-evaluating resting-state SEEG functional connectivity over distance in subjects with Engel I versus Engel II–IV surgical outcomes, we observed that PZs exhibited the largest identifiable difference in connectivity profiles. Specifically, PZs exhibit an intermediate connectivity profile to that of SOZs and NIZs in subjects with Engel I outcomes (Fig. 6; two-way repeated measures ANOVA group effect $P = 1.16 \times 10^{-2}$, distance effect-value $= 1.26 \times 10^{-2}$, interaction $P = 5.15 \times 10^{-2}$). Conversely, PZ 95% confidence intervals become indistinguishable from NIZs and significantly different from SOZs for subjects with Engel II–IV outcomes (Fig. 6B; two-way repeated measures ANOVA group effect $P = 1.73 \times 10^{-4}$, distance effect $P = 7.83 \times 10^{-1}$, interaction $P = 3.01 \times 10^{-3}$). Finally, the mean variance of SOZ versus PZ reciprocal connectivity was 0.414 for Engel I and 0.280 for Engel II–IV (two-sample t-test $P = 0.394$), indicating that PZ connectivity in Engel II–IV subjects was not only lower, but also more consistently

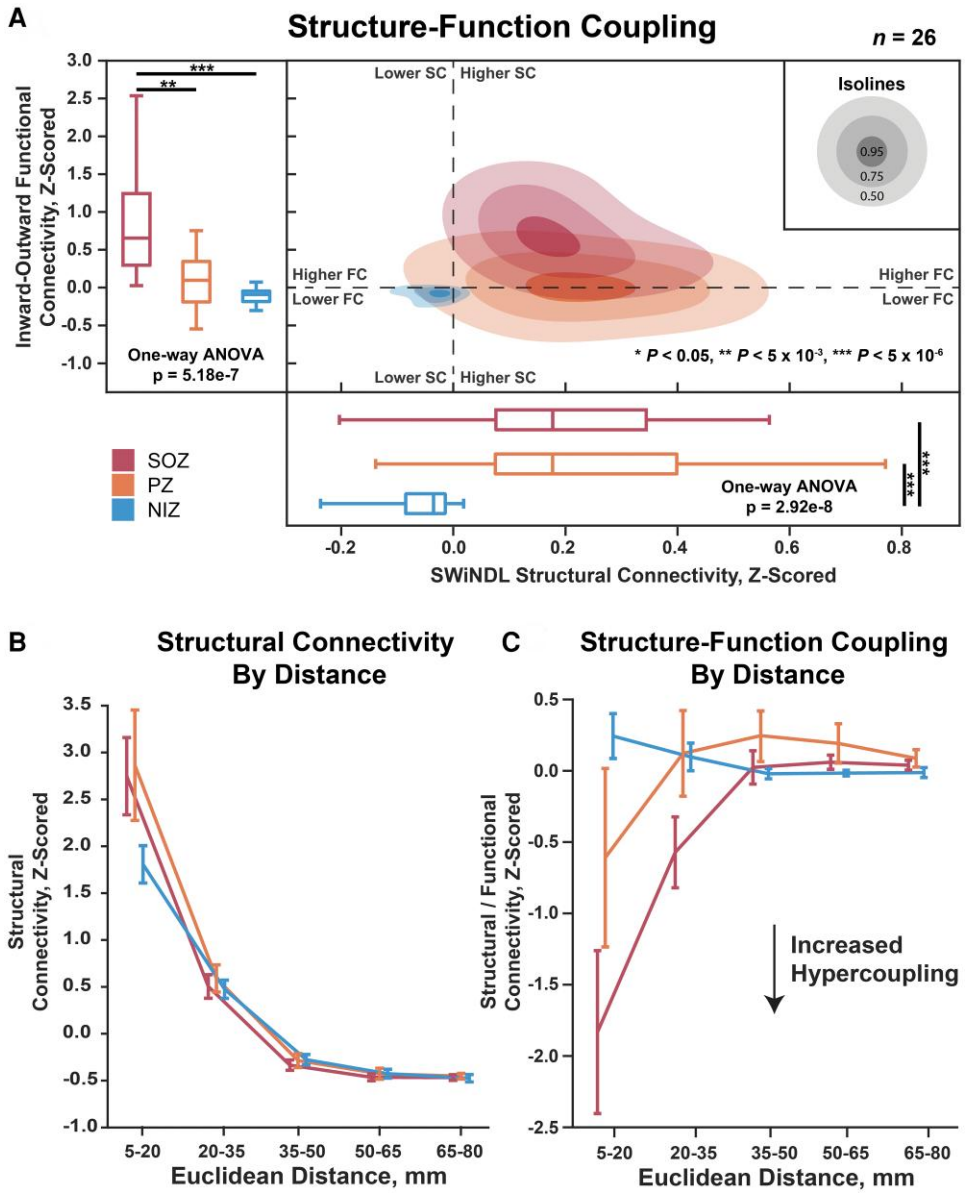

Figure 5 Structure–function coupling over Euclidean distance. (**A**) The left boxplots show the functional connectivity (PDC inwards strength minus outwards strength) of SOZ, PZ and NIZ. The bottom boxplots show structural connectivity as measured by SWiNDL. The contours in the middle show the 2D distribution of the scatterplot of functional versus structural connectivity. (**B**) Structural connectivity over Euclidean edge distance. Error bars represent 95% confidence intervals. Repeated measures two-way ANOVA: SOZ/PZ/NIZ effect $P = 7.52 \times 10^{-3}$, distance effect $P = 1.75 \times 10^{-64}$, interaction effect $P = 5.44 \times 10^{-9}$. (**C**) Structural–functional connectivity over Euclidean edge distance. Repeated measures two-way ANOVA: SOZ/PZ/NIZ effect $P = 7.27 \times 10^{-4}$, distance effect $P = 8.63 \times 10^{-19}$, interaction effect $P = 9.76 \times 10^{-21}$. Post-ANOVA multiple comparison: $^{**}P < 5 \times 10^{-3}$, $^{***}P < 5 \times 10^{-6}$. $n = 26$ patients.

resembled NIZ connectivity compared to Engel I subjects. These results could indicate a fundamental difference of PZ connectivity in subjects with Engel II–IV surgical outcome or could reflect different SEEG sampling and subsequently different ictal event interpretation in these subjects.

A structure–function coupling model most accurately classifies SEEG nodes as SOZ, PZ or NIZ

Using a nested cross-validation model (Fig. 7A), we first trained an SVM with only the resting-state SEEG functional connectivity data summarized in Fig. 2 to classify individual SEEG nodes as residing in an SOZ, PZ or NIZ (Fig. 7B). The model achieved an overall accuracy of 84.4% (±2.1% SD) and individual true positive rates of 92.0 ± 6.9% for SOZs, 81.6 ± 5.4% for PZs and 53.0 ± 1.8% for NIZs. Incorporating SWiNDL structural connectivity derived from DWI data into the model raised the test set overall accuracy to 92.0 ± 2.2% and the individual true positive rates to 92.5 ± 7.2% for SOZs, 93.0 ± 5.3% for PZs and 71.2 ± 2.0% for NIZs (Fig. 7C).

We then sought to test the accuracy of a functional connectivity model only trained on Engel I outcome subjects (Fig. 7D). For this model, the test set overall model accuracy increased compared to the accuracy for the entire cohort to 89.5 ± 2.8%, with true positive rate increasing for PZ and NIZs, but remaining unchanged for SOZs. Next, when using the Engel I model on Engel II–IV subjects, the accuracies dropped to a mean of 67.1 ± 0.4%. Overall, these

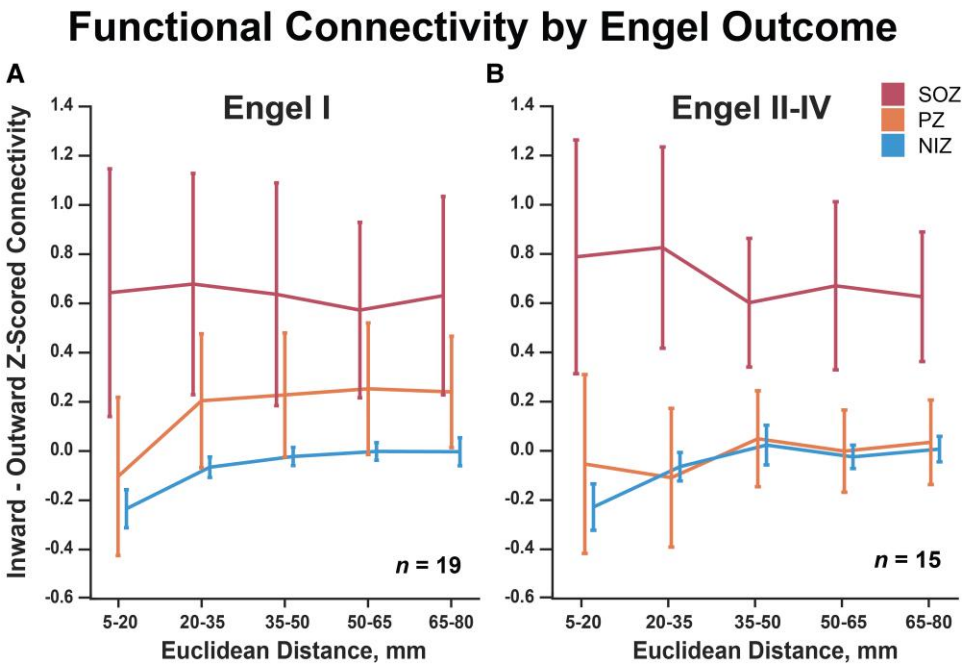

Figure 6 Functional connectivity by Engel outcome. (**A**) SOZ, PZ and NIZ connectivity for subjects with Engel 1 outcomes (two-way repeated measures ANOVA group effect $P = 1.16 \times 10^{-2}$, distance effect $P = 1.26 \times 10^{-2}$, interaction $P = 5.15 \times 10^{-2}$). (**B**) PZs exhibit lower connectivity in subjects with Engel II–IV outcomes (two-way repeated measures ANOVA group effect $P = 1.73 \times 10^{-4}$, distance effect $P = 7.83 \times 10^{-1}$, interaction $P = 3.01 \times 10^{-3}$). Error bars represent 95% confidence intervals of the mean.

findings suggest that a model trained on readily available resting-state SEEG data can accurately classify SOZs, PZs and NIZs, but accuracy increases if DWI data are available. Furthermore, the large drop in accuracy when using the Engel I model on Engel II–IV subjects could suggest that Engel II–IV subjects have a fundamentally different connectivity profile to that of subjects who achieved Engel I outcomes. Alternatively, this drop in model performance could be attributed to clinically defined SOZ (and thus potential EZs) being more likely to be inaccurate in patients with Engel II–IV outcomes.

Discussion

The concept of excitation and inhibition in epilepsy has been investigated for decades.[29,80–82] Specifically, at the cellular level, GABA signalling is thought to play a pivotal role in seizure initiation and termination when investigated *in vitro*, *ex vivo* and with optogenetics.[83–85] When abstracted to electrographic networks, the concept of inhibition and excitation has been explored as it relates to inwards and outwards connectivity of epileptogenic zones. Recent evidence has suggested that epileptogenic zones have increased inwards connectivity, which could relate to interictal suppression of epileptiform activity[19,20,27,34,39,40,86–88]; whereas other works have focused on observations of increased outwards connectivity from SOZs to the rest of the network.[31,37,89] In response to the existing variety of observations and interpretations of functional connectivity in the epileptic network, this work sought to partially test the specific hypothesis of interictal suppression of SOZs (the ISH) at the electrographic network level by characterizing the direction and relative elevation or attenuation of neural activity.

Properly testing the ISH with only resting-state SEEG connectivity is challenging due to the difficulty of interpreting whether resting-state functional connectivity is excitatory, inhibitory or neutral. For example, increased inwards connectivity could be interpreted with known directed connectivity motifs,[90] but it will not directly indicate if this increase in inwards connectivity correlates to any region being suppressed or excited. Thus, we conducted SPES to (i) provide additional insight into the directionality of network connectivity with another paradigm; and (ii) quantify elevation or attenuation of frequency-band power by measuring the change in relative band power from the prestimulation baseline. Using SPES, we can gain insight into the potential excitatory and inhibitory nature of the network connectivity. However, it is important to consider that SPES itself may be altering the network dynamics away from the resting state. Thus, interpretation of resting-state SEEG and SPES findings must be carefully integrated.

Further complicating this discussion, one cannot assume that attenuation in a certain frequency-band power aligns with inhibition. As an example, there is a large body of evidence that an increase in beta power correlates to inhibition of motor circuits, particularly in Parkinson's disease.[91,92] For the sake of clarity, we will use the term 'elevation' to refer to an increase in signal band power, and 'attenuation' to refer to a decrease. We will reserve the terms 'excitation' and 'inhibition/suppression' for the concept of how a modification in neural activity relates to a change in a clinically observable behaviour of interest (e.g. seizure versus no seizure). Furthermore, we use the term 'seizure-onset zone' to indicate an area of first observed electrographic epileptiform changes. We reserve the use of the term 'epileptogenic zone' (i.e. 'site of the beginning of the epileptic seizures and of their primary organization') for discussion of an electroclinically defined region that must be resected to render the subject seizure free and typically contains an SOZ.[10] Finally, a hinderance to meaningful comparison of studies across research groups is the variety of brain atlases to segment the brain for connectivity analyses.[49] Thus, we have implemented a series of electrographic and structural analyses that do not rely on any atlas parcellations. With these considerations and definitions in mind, we will discuss our interpretation of the pertinent findings in this work.

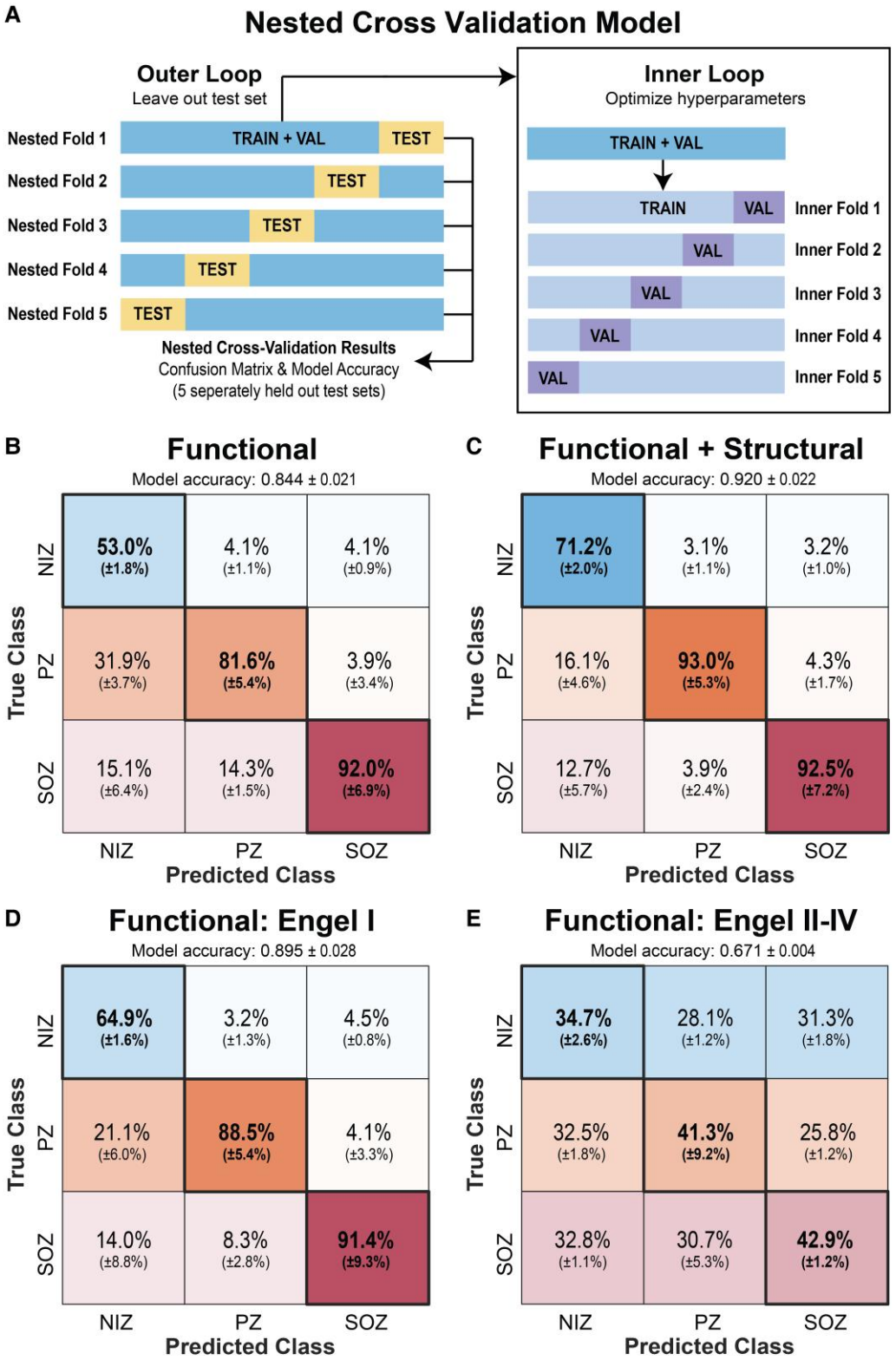

Figure 7 Classification of SOZ, PZ and NIZs using an SVM. (**A**) A 5-fold nested cross-validation scheme was used to evaluate the SVM's ability to classify SOZ versus PZ versus NIZ. A completely withheld testing set delineated at the patient level was used for each model evaluation. (**B**) Confusion matrix when only functional connectivity was used to generate the model. Overall held-out test set accuracy of 84.4 ± 2.1% (mean ± SD). Confusion matrix percentages are normalized by column—i.e. each confusion matrix entry can be interpreted as 'If the model predicts this SEEG contact is a [SOZ/PZ/NIZ], then there is an X% chance it truly is'. (**C**) Confusion matrix for a model using functional and structural connectivity with overall held-out test set accuracy of 0.920 ± 2.2%. (**D**) Confusion matrix for a model generated with only Engel I subjects with overall held-out test set accuracy of 89.5 ± 2.8% (**E**) Confusion matrix for Engel II–IV subjects tested with the model generated from Engel I subjects (i.e. model 'D') with overall held-out test set accuracy of 67.1 ± 0.4%.

Does imbalanced reciprocal connectivity indicate suppression?

In this study, we observed imbalanced reciprocal (inwards–outwards) connectivity of SOZs and PZs: specifically, SOZs demonstrated a large increase in inwards connectivity and a moderate decrease in outwards connectivity in resting-state SEEG analyses. These results are consistent across all frequency bands for directed connectivity. PZs showed a similar imbalance in reciprocal connectivity to SOZs, but to an intermediate extent. Important for interpretation, NIZ reciprocal connectivity was approximately zero —i.e. regions not directly involved in seizure onset or early propagation have roughly equal inwards and outwards connectivity. This suggests that SOZs and PZs interact with the network differently than presumably healthy regions of the brain. One interpretation of this finding is that SOZs are actively isolated or segregated by other regions of the brain. It is possible that healthy regions are sending inhibitory signals to the SOZs and PZs (increased inwards connectivity) and thus suppress their ability to communicate with the rest of the network and initiate seizures (decreased outwards connectivity).

Further evidence for SOZ segregation was exhibited in the reciprocal connectivity elucidated with low-frequency stimulation. First, it is important to note that our PSD approach is fundamentally different than metrics that rely on cortico-cortical evoked potential waveform morphology. Specifically, evoked potentials can be difficult to interpret with depth electrodes due to the inconsistency of evoked potential amplitude due to orientation uncertainty relative to pyramidal neurons.[30,40–44] These methodological differences are important to interpret our PSD approaches compared to evoked potential approaches that may initially appear to show conflicting results.[93] Overall, when presumably healthy regions were stimulated, the SOZ theta (4–8 Hz) relative band power was markedly decreased from prestimulation baseline. Conversely, SOZ beta (13–30 Hz), low-gamma (31–80 Hz) and high-gamma (81–150 Hz) relative band power increased when healthy regions were stimulated. Increased inwards evoked gamma band power in SOZs is in alignment with previous low-frequency stimulation findings.[34] Notably, reciprocal evoked alpha-band power was not altered across all region designations, and PZ relative band power was not significantly altered for any frequency band measured.

It has been long known that theta spectral power accounts for a significantly larger portion of whole-band power on EEG recordings compared to beta and gamma power.[94] Additionally, theta power is thought to be involved with long-range integration of brain regions, whereas gamma power is considered important for local integration.[95–97] Thus, simultaneous attenuation of a high-power spectral band (theta), in parallel with excitation of a locally integrating frequency band (gamma), suggests that SOZ functional segregation is increased when NIZs are stimulated. Furthermore, gamma activity is thought to reflect GABA inhibitory interneuron activity.[98–100] Thus, increased inwardly activated gamma band power in SOZs could reflect a direct change in the GABA interneuron balance. Furthermore, important to consider is that gamma activity, in the form of low-voltage fast activity, is commonly observed on intracranial EEG immediately before ictal onset and increased baseline gamma power is thought to be a biomarker for the 'ictal core'.[101–103] Thus, it is possible that the observed SOZ increase in gamma power when non-SOZ nodes are stimulated is simply SOZs demonstrating an enhancement of an intrinsic pathologically distinct phenomenon and could actually be driving SOZs towards an ictal state. To further detail this discussion, it is important to integrate previous works that argue 'low-gamma oscillations' but not 'broad-band high-gamma activities (not oscillations)' are involved in GABAergic inhibition.[99,104] In this regard, the argument of network inhibition is complicated by the fact that both low-gamma (reflecting GABA activities in the presence of oscillations) and high-gamma (proxy of neuronal firing) power are elevated in SOZs when non-SOZs are stimulated at low frequencies. Finally, previous work has shown that poststimulation SOZ decrease in low-frequency power and increase in high-frequency power correlates to favourable surgical outcome.[105] It is difficult to disentangle stimulation-induced changes in low- and high-frequency spectral power of SOZs due to the complex biophysical origin of spectral power within the brain. The direct source of the changes in spectral power remains unknown and the current evidence is not sufficient to completely test the ISH. Overall, the SPES findings simply provide evidence for an electrographic network-level increase in inwards connectivity to the SOZ and can provide insight into the frequency-specific behaviour of SOZs during stimulation, but more work is needed to further test the ISH.

Reciprocal connectivity is edge distance invariant, but SOZs exhibit local structure–function hypercoupling

We sought to investigate whether findings of increased inwards connectivity to SOZs were affected by Euclidean distance and/or estimates of anatomical white-matter connectivity between SEEG contacts. Past work has demonstrated the importance of considering Euclidean edge distance when analysing functional epileptogenic networks.[106] Specifically, it has been demonstrated that short-range structural connections drive most of the aberrant SOZ connectivity and could dictate seizure spread.[19,107,108] This observation of rapid functional connectivity decay with increasing edge length was recapitulated in this work's undirected and directed resting-state findings. However, long-range connections are thought to add diversity and complexity to brain networks and could be important contributors to widescale integration.[109] Concordantly, our finding that resting-state reciprocal connectivity is relatively constant across distance suggests that distant brain regions may still play an important role in SOZ excitation and inhibition.

Beyond simple Euclidean distance metrics, diffusion-derived structural connectivity characteristics can be used to investigate potential pathological SOZ connectivity.[110–116] We saw that SOZs and PZs to have increased structural connectivity relative to NIZs, which is in alignment with past SEEG-informed diffusion imaging studies.[111] This increase could represent an intrinsic pathological biomarker of the epileptogenic network or could possibly be due to implantation bias increasing the density of SEEG contacts around suspected SOZs. Of more pertinent interest to testing the ISH, we investigated whether structural connectivity variation could explain our observed differences in functional connectivity. The 'coupling' between structure and function is the term commonly used when the strength of structural connections predicts the strength of functional connections.[117] Thus, a region exhibits strong structure–function coupling when the ratio of their relative functional and structural connections is unity. We use the term 'hypercoupling' to refer to connections that exceed the functional connection strength expected from structural connectivity. We observed that SOZs demonstrate markedly increased local hypercoupling—i.e. the increased inwards functional connectivity strength is disproportionally elevated above the average structure–function

coupling by two standard deviations for edge connections within 5–20 mm. This suggests an abnormal functional reorganization around the SOZs disproportionate to any alterations in structural connectivity.

Proper propagation zone identification may help prognosticate surgical outcome

A subanalysis with Engel I versus Engel II–IV surgical resection outcomes demonstrated that PZ connectivity resembled NIZ connectivity in Engel II–IV subjects. This could be due to an intrinsic difference in SOZ/PZ connectivity between surgical responders and non-responders (perhaps a difference in focality of SOZs for surgical responders), a difference in SEEG implantation strategy between the patient groups that affects network observations or a difference in ictal interpretation that affects node designation.[47,118,119] With this observation as motivation, we developed SVM models to classify SOZs, PZs and NIZs. The models were able to classify SOZs with very high accuracy (range of 91.4–92.5% accuracy) but differed in ability to differentiate PZs from NIZs (range of 81.6–93.0% accuracy). Notably, our SVM model to classify individual SEEG bipolar pairs confused PZs and NIZs when the entire subject cohort was used in model generation and testing (31.9% false identification of PZs as NIZs). When restricted to Engel I subjects, the model improved classification between PZs and NIZs, with subsequently very poor performance when this model was used to test Engel II–IV subjects. Of note, the best model was produced when diffusion-derived metrics were included, but these data are less commonly collected during presurgical workup. Overall, the models very accurately classified SOZs, but we encourage other groups to include PZ classification into model design because it may be an important factor for prognosticating surgical outcome.

Alternative interpretations of existing evidence and limitations

This work uses multiple analysis techniques to test the ISH but is limited by the ambiguity of network neuroscience interpretation and integration. Electrographic phenomena observed on SEEG and probabilistic tractography performed on diffusion imaging are removed from underlying neurophysiology and neuropathology. Thus, interpretation of functional and structural network connectivity findings must resist the proclivity towards self-justified and circular conclusions. Further complicating interpretation is the lack of control groups for these populations because SEEG control data does not exist. All scientific inferences and hypothesis testing were conducted on comparisons to regions presumably not involved in the genesis or early propagation of epileptiform activity. For subjects with epilepsy, it could be reasonable to assume that the entire brain network is sick and thus intra-patient normalization to 'healthy' regions could be an ill-posed analytical model. As more depth electrodes are being used for therapy in people with varying psychiatric and neurological disorders, large-scale data sharing to expand our understanding of baseline electrographic phenomena across a more diverse population could help address these issues.

Important to discuss are interpretations of the existing data that are at odds with the ISH. It is possible that the observed increase in inwards and decrease in outwards connectivity are not actually suggestive of suppression. For example, the increase in inwards connections could be a long-term activating signal that eventually pushes the SOZs past a critical threshold to cause a seizure. Another interpretation could be that the decreased outwards connectivity of SOZs represents an SOZ segregation that enables seizure origination because a healthier integration with surrounding brain regions would actually lead to suppression. Due to the complexity of understanding brain networks, multiple explanations to these data are possible and it is important to balance our interpretations.

Beyond potential interpretation differences, methodological limitations to discuss include the assignment of SOZ/PZ/NIZ labels, SEEG interictal epileptiform events, stimulation parameters and structure–function coupling assumptions. Specifically, epileptologist variability in seizure annotations could lead to varied SOZ/PZ/NIZ assignment. An alternative approach with multiple new epileptologists that each review all seizure events with formal disagreement protocols could help address this limitation. Furthermore, the definition of PZs to be within 10 s of observed ictal onset does not allow for individual patient differences in propagation patterns and could be an oversimplification of real ictal dynamics. Regarding interictal epileptiform events, we made the decision to avoid potentially biased manual segmentation of the resting-state SEEG to reject possible discharges in favour of averaging the results of multiple 2-min raw epochs to capture the variability of network connectivity. However, this approach could introduce mathematical eccentricities in the connectivity calculations with high amplitude discharges and is an important limitation to consider. Next, a single stimulation paradigm was used for SPES and jittering was not applied to the electrical stimulus during SPES to mitigate possible entrainment effects that could lead to power changes. Ideally, implementing multiple SPES protocols would help address these limitations, but practical data collection limitations such as time, clinical workflow and patient tolerance need to be considered. Finally, one assumption made about the phenomenon of 'hypercoupling' is that it occurs when functional connectivity exceeds structural connectivity between two nodes. However, the hypercoupling phenomenon may simply reflect functional connectivity that is a result of indirect structural paths or routes across the network. Structural connectivity metrics such as 'search information' incorporate all possible structural paths between nodes into the connectivity metric and may help resolve the contributions of indirect structural connections towards functional connectivity.[120]

Conclusions

In summary, using resting-state SEEG analyses and low-frequency stimulation, we observed electrographic evidence that could support the hypothesis of interictal functional suppression of SOZs and PZs. When controlling for distance and structural connectivity, we found that SOZs and PZs demonstrate consistent long-range relative reciprocal connectivity, but elevated local hypercoupling of functional connectivity that could indicate enhanced local interictal suppression of SOZs. Finally, we have demonstrated that a clinically useful model can be generated using only SEEG data to classify SOZs, PZs and NIZs. However, inclusion of DWI-derived structural connectivity can increase the model accuracy. Overall, we believe this work supports the hypothesis of interictal suppression of SOZs and could have practical implications to reduce the morbidity of the presurgical workup and aid clinical decision making for this devastating neurological disorder.

Acknowledgements

We would like to thank the patients for participating in this investigation.

Funding

This work was supported by the following funding sources: NINDS R00-NS097618, NINDS R01-NS112252, NINDS R01-NS075270, NINDS R01-NS110130, NINDS R01-NS108445, NINDS R01-NS095291, NINDS F31-NS120401 and National Institutes of Health Training Grants: NIGMS T32-GM007347, NIBIB T32-EB021937 and NIBIB T32-EB001628.

Competing interests

The authors report no competing interests.

Supplementary material

Supplementary material is available at *Brain* online.

References

1. Behr C, Goltzene MA, Kosmalski G, Hirsch E, Ryvlin P. Epidemiology of epilepsy. *Rev Neurol (Paris)*. 2016;172:27-36.
2. Engel J Jr. What can we do for people with drug-resistant epilepsy? The 2016 Wartenberg Lecture. *Neurology*. 2016;87:2483-2489.
3. Englot DJ, Chang EF. Rates and predictors of seizure freedom in resective epilepsy surgery: An update. *Neurosurg Rev*. 2014;37:389-405; discussion 404-5.
4. Engel J, McDermott MP, Wiebe S, *et al*. Early surgical therapy for drug-resistant temporal lobe epilepsy: A randomized trial. Multicenter study randomized controlled trial research support, N.I.H., extramural. *JAMA*. 2012;307:922-930.
5. Wu C, Jermakowicz WJ, Chakravorti S, *et al*. Effects of surgical targeting in laser interstitial thermal therapy for mesial temporal lobe epilepsy: A multicenter study of 234 patients. *Epilepsia*. 2019;60:1171-1183.
6. Wicks RT, Jermakowicz WJ, Jagid JR, *et al*. Laser interstitial thermal therapy for mesial temporal lobe epilepsy. *Neurosurgery*. 2016;79(Suppl 1):S83-S91.
7. Englot DJ, Birk H, Chang EF. Seizure outcomes in nonresective epilepsy surgery: An update. *Neurosurg Rev*. 2017;40:181-194.
8. Boon P, De Cock E, Mertens A, Trinka E. Neurostimulation for drug-resistant epilepsy: A systematic review of clinical evidence for efficacy, safety, contraindications and predictors for response. *Curr Opin Neurol*. 2018;31:198-210.
9. Parvizi J, Kastner S. Promises and limitations of human intracranial electroencephalography. *Nat Neurosci*. 2018;21:474-483.
10. Kahane P, Landré E, Minotti L, Francione S, Ryvlin P. The Bancaud and Talairach view on the epileptogenic zone: A working hypothesis. *Epileptic Disord*. 2006;8:S16-S26.
11. Khoo HM, Hall JA, Dubeau F, *et al*. Technical aspects of SEEG and its interpretation in the delineation of the epileptogenic zone. *Neurol Med Chir (Tokyo)*. 2020;60:565–5580.
12. Rheims S, Ryvlin P. Patients' safety in the epilepsy monitoring unit: Time for revising practices. *Curr Opin Neurol*. 2014;27:213-218.
13. Karthick P, Tanaka H, Khoo HM, Gotman J. Could we have missed out the seizure onset: A study based on intracranial EEG. *Clin Neurophysiol*. 2020;131:114-126.
14. Cimbalnik J, Klimes P, Sladky V, *et al*. Multi-feature localization of epileptic foci from interictal, intracranial EEG. *Clin Neurophysiol*. 2019;130:1945-1953.
15. Taylor PN, Papasavvas CA, Owen TW, *et al*. Normative brain mapping of interictal intracranial EEG to localize epileptogenic tissue. *Brain*. 2022;145:939–949.
16. Weiss SA, Staba RJ, Sharan A, *et al*. Accuracy of high-frequency oscillations recorded intraoperatively for classification of epileptogenic regions. *Sci Rep*. 2021;11:1–12.
17. Frauscher B. Localizing the epileptogenic zone. *Curr Opin Neurol*. 2020;33:198-206.
18. Balaji SS, Parhi KK. Seizure onset zone identification from iEEG: A review. *IEEE Access*. 2022;10:62535-62547.
19. Goodale SE, González HFJ, Johnson GW, *et al*. Resting-state SEEG may help localize epileptogenic brain regions. *Neurosurgery*. 2020;86:792-801.
20. Narasimhan S, Kundassery KB, Gupta K, *et al*. Seizure-onset regions demonstrate high inward directed connectivity during resting-state: An SEEG study in focal epilepsy. *Epilepsia*. 2020;61:2534-2544.
21. Foit NA, Bernasconi A, Bernasconi N. Functional networks in epilepsy presurgical evaluation. *Neurosurg Clin N Am*. 2020;31:395-405.
22. Larivière S, Bernasconi A, Bernasconi N, Bernhardt BC. Connectome biomarkers of drug-resistant epilepsy. *Epilepsia*. 2021;62:6-24.
23. Royer J, Bernhardt BC, Larivière S, *et al*. Epilepsy and brain network hubs. *Epilepsia*. 2022;63:537–550.
24. Stacey W, Kramer M, Gunnarsdottir K, *et al*. Emerging roles of network analysis for epilepsy. *Epilepsy Res*. 2020;159:106255.
25. Johnson GW, Doss DJ, Englot DJ. Network dysfunction in pre and postsurgical epilepsy: Connectomics as a tool and not a destination. *Curr Opin Neurol*. 2022;35:196-201.
26. Sinha N, Johnson GW, Davis KA, Englot DJ. Integrating network neuroscience into epilepsy care: Progress, barriers, and next steps. *Epilepsy Currents*. 2022;22:272-278.
27. Gunnarsdottir KM, Gonzalez-Martinez J, Wing S, Sarma SV. *Sources and sinks in interictal iEEG networks: An iEEG marker of the epileptogenic zone*. IEEE; 2021.
28. Pavlov I, Walker MC. Tonic GABA(A) receptor-mediated signalling in temporal lobe epilepsy. *Neuropharmacology*. 2013;69:55-61.
29. Engel J. Excitation and inhibition in epilepsy. *Canadian Journal of Neurological Sciences/Journal Canadien des Sciences Neurologiques*. 1996;23:167-174.
30. Valentin A, Anderson M, AlarcoÂn G, *et al*. Responses to single pulse electrical stimulation identify epileptogenesis in the human brain in vivo. *Brain*. 2002;125:1709-1718.
31. Matsumoto R, Kunieda T, Nair D. Single pulse electrical stimulation to probe functional and pathological connectivity in epilepsy. *Seizure*. 2017;44:27-36.
32. Flanagan D, Valentín A, García Seoane JJ, Alarcón G, Boyd SG. Single-pulse electrical stimulation helps to identify epileptogenic cortex in children. *Epilepsia*. 2009;50:1793-1803.
33. Boido D, Kapetis D, Gnatkovsky V, *et al*. Stimulus-evoked potentials contribute to map the epileptogenic zone during stereo-EEG presurgical monitoring. *Hum Brain Mapp*. 2014;35:4267-4281.
34. Kundu B, Davis TS, Philip B, *et al*. A systematic exploration of parameters affecting evoked intracranial potentials in patients with epilepsy. *Brain Stimul*. 2020;13:1232-1244.
35. Mouthaan BE, Van'T Klooster MA, Keizer D, *et al*. Single pulse electrical stimulation to identify epileptogenic cortex: Clinical information obtained from early evoked responses. *Clin Neurophysiol*. 2016;127:1088-1098.
36. Van'T Klooster MA, Zijlmans M, Leijten FSS, Ferrier CH, Van Putten MJAM, Huiskamp GJM. Time–frequency analysis of single pulse electrical stimulation to assist delineation of epileptogenic cortex. *Brain*. 2011;134:2855-2866.

37. Guo Z-h, Zhao B-t, Toprani S, *et al*. Epileptogenic network of focal epilepsies mapped with cortico-cortical evoked potentials. *Clin Neurophysiol*. 2020;131:2657-2666.
38. Prime D, Woolfe M, Rowlands D, O'Keefe S, Dionisio S. Comparing connectivity metrics in cortico-cortical evoked potentials using synthetic cortical response patterns. *J Neurosci Methods*. 2020;334:108559.
39. Zhang N, Zhang B, Rajah GB, *et al*. The effectiveness of cortico-cortical evoked potential in detecting seizure onset zones. *Neurol Res*. 2018;40:480-490.
40. Parker CS, Clayden JD, Cardoso MJ, *et al*. Structural and effective connectivity in focal epilepsy. *Neuroimage Clin*. 2018;17:943-952.
41. Matsumoto R, Nair DR, LaPresto E, Bingaman W, Shibasaki H, Luders HO. Functional connectivity in human cortical motor system: A cortico-cortical evoked potential study. *Brain*. 2006; 130(Pt 1):181-197.
42. van Blooijs D, Leijten FSS, van Rijen PC, Meijer HGE, Huiskamp GJM. Evoked directional network characteristics of epileptogenic tissue derived from single pulse electrical stimulation. *Hum Brain Mapp*. 2018;39:4611-4622.
43. Paulk AC, Zelmann R, Crocker B, *et al*. Local and distant cortical responses to single pulse intracranial stimulation in the human brain are differentially modulated by specific stimulation parameters. *Brain Stimul*. 2022;15:491-508.
44. Prime D, Rowlands D, O'Keefe S, Dionisio S. Considerations in performing and analyzing the responses of cortico-cortical evoked potentials in stereo-EEG. *Epilepsia*. 2018;59:16-26.
45. Crocker B, Ostrowski L, Williams ZM, *et al*. Local and distant responses to single pulse electrical stimulation reflect different forms of connectivity. *Neuroimage*. 2021;237:118094.
46. D'Haese P-F, Pallavaram S, Li R, *et al*. Cranialvault and its CRAVE tools: A clinical computer assistance system for deep brain stimulation (DBS) therapy. *Med Image Anal*. 2012;16: 744-753.
47. Andrews JP, Gummadavelli A, Farooque P, *et al*. Association of seizure spread with surgical failure in epilepsy. *JAMA Neurol*. 2019;76:462.
48. Engel J. Update on surgical treatment of the epilepsies: Summary of the second international palm desert conference on the surgical treatment of the epilepsies (1992). *Neurology*. 1993;43:1612-1612.
49. Revell AY, Silva AB, Arnold TC, *et al*. A framework for brain atlases: Lessons from seizure dynamics. *Neuroimage*. 2022;254:118986.
50. Sekihara K, Owen JP, Trisno S, Nagarajan SS. Removal of spurious coherence in MEG source-space coherence analysis. *IEEE Trans Biomed Eng*. 2011;58:3121-3129.
51. Rolston JD, Chang EF. Critical language areas show increased functional connectivity in human cortex. *Cerebral Cortex*. 2018;28:4161-4168.
52. Englot DJ, Hinkley LB, Kort NS, *et al*. Global and regional functional connectivity maps of neural oscillations in focal epilepsy. *Brain*. 2015;138:2249-2262.
53. Hinkley LBN, Marco EJ, Findlay AM, *et al*. The role of corpus callosum development in functional connectivity and cognitive processing. *PLoS ONE*. 2012;7:e39804.
54. Prime D, Woolfe M, O'Keefe S, Rowlands D, Dionisio S. Quantifying volume conducted potential using stimulation artefact in cortico-cortical evoked potentials. *J Neurosci Methods*. 2020;337:108639.
55. Tournier JD, Smith R, Raffelt D, *et al*. MRtrix3: A fast, flexible and open software framework for medical image processing and visualisation. *NeuroImage*. 2019;202:116137.
56. Jenkinson M, Beckmann CF, Behrens TEJ, Woolrich MW, Smith SM. FSL. *NeuroImage*. 2012;62:782-790.
57. Tustison NJ, Cook PA, Klein A, *et al*. Large-scale evaluation of ANTs and FreeSurfer cortical thickness measurements. *NeuroImage*. 2014;99:166-179.
58. Cai LY, Yang Q, Hansen CB, *et al*. Prequal: An automated pipeline for integrated preprocessing and quality assurance of diffusion weighted MRI images. *Magn Reson Med*. 2021;86:456-470.
59. Veraart J, Novikov DS, Christiaens D, Ades-Aron B, Sijbers J, Fieremans E. Denoising of diffusion MRI using random matrix theory. *NeuroImage*. 2016;142:394-406.
60. Veraart J, Fieremans E, Novikov DS. Diffusion MRI noise mapping using random matrix theory. *Magn Reson Med*. 2016;76: 1582-1593.
61. Cordero-Grande L, Christiaens D, Hutter J, Price AN, Hajnal JV. Complex diffusion-weighted image estimation via matrix recovery under general noise models. *NeuroImage*. 2019;200: 391-404.
62. Schilling KG, Blaber J, Hansen C, *et al*. Distortion correction of diffusion weighted MRI without reverse phase-encoding scans or field-maps. *PLoS ONE*. 2020;15:e0236418.
63. Andersson JL, Skare S, Ashburner J. How to correct susceptibility distortions in spin-echo echo-planar images: Application to diffusion tensor imaging. *Neuroimage*. 2003;20:870-888.
64. Smith SM, Jenkinson M, Woolrich MW, *et al*. Advances in functional and structural MR image analysis and implementation as FSL. *Neuroimage*. 2004;23(Suppl 1):S208-S219.
65. Andersson JLR, Sotiropoulos SN. An integrated approach to correction for off-resonance effects and subject movement in diffusion MR imaging. *Neuroimage*. 2016;125:1063-1078.
66. Andersson JLR, Graham MS, Zsoldos E, Sotiropoulos SN. Incorporating outlier detection and replacement into a non-parametric framework for movement and distortion correction of diffusion MR images. *Neuroimage*. 2016;141:556-572.
67. Smith RE, Tournier J-D, Calamante F, Connelly A. SIFT2: Enabling dense quantitative assessment of brain white matter connectivity using streamlines tractography. *NeuroImage*. 2015;119:338-351.
68. Iglesias JE, Cheng-Yi L, Thompson PM, Zhuowen T. Robust brain extraction across datasets and comparison with publicly available methods. *IEEE Trans Med Imaging*. 2011;30:1617-1634.
69. Tustison NJ, Avants BB, Cook PA, *et al*. N4ITK: Improved N3 bias correction. *IEEE Trans Med Imaging*. 2010;29:1310-1320.
70. Bhushan C, Haldar JP, Choi S, Joshi AA, Shattuck DW, Leahy RM. Co-registration and distortion correction of diffusion and anatomical images based on inverse contrast normalization. *Neuroimage*. 2015;115:269-280.
71. Zhang Y, Brady M, Smith S. Segmentation of brain MR images through a hidden Markov random field model and the expectation-maximization algorithm. *IEEE Trans Med Imaging*. 2001;20:45-57.
72. Smith SM. Fast robust automated brain extraction. *Hum Brain Mapp*. 2002;17:143-155.
73. Patenaude B, Smith SM, Kennedy DN, Jenkinson M. A Bayesian model of shape and appearance for subcortical brain segmentation. *NeuroImage*. 2011;56:907-922.
74. Tournier JD, Calamante F, Gadian DG, Connelly A. Direct estimation of the fiber orientation density function from diffusion-weighted MRI data using spherical deconvolution. *NeuroImage*. 2004;23:1176-1185.
75. Jeurissen B, Tournier J-D, Dhollander T, Connelly A, Sijbers J. Multi-tissue constrained spherical deconvolution for improved analysis of multi-shell diffusion MRI data. *NeuroImage*. 2014;103:411-426.
76. Tournier J-D, Calamante F, Connelly A. Improved probabilistic streamlines tractography by 2nd order integration over fibre

orientation distributions. *Proceedings of the International Society for Magnetic Resonance in Medicine*. ISMRM; 2009.
77. Smith RE, Tournier J-D, Calamante F, Connelly A. Anatomically-constrained tractography: Improved diffusion MRI streamlines tractography through effective use of anatomical information. *NeuroImage*. 2012;62:1924-1938.
78. Smith RE, Tournier J-D, Calamante F, Connelly A. The effects of SIFT on the reproducibility and biological accuracy of the structural connectome. *NeuroImage*. 2015;104:253-265.
79. Kajikawa Y, Schroeder CE. How local is the local field potential? *Neuron*. 2011;72:847-858.
80. Scharfman HE. The neurobiology of epilepsy. *Curr Neurol Neurosci Rep*. 2007;7:348-354.
81. Naylor DE. Glutamate and GABA in the balance: Convergent pathways sustain seizures during status epilepticus. *Epilepsia*. 2010;51:106-109.
82. Shao L-R, Habela CW, Stafstrom CE. Pediatric epilepsy mechanisms: Expanding the paradigm of excitation/inhibition imbalance. *Children*. 2019;6:23.
83. Treiman DM. GABAergic mechanisms in epilepsy. *Epilepsia*. 2001;42:8-12.
84. Krook-Magnuson E, Armstrong C, Oijala M, Soltesz I. On-demand optogenetic control of spontaneous seizures in temporal lobe epilepsy. *Nat Commun*. 2013;4:1376.
85. Ledri M, Madsen MG, Nikitidou L, Kirik D, Kokaia M. Global optogenetic activation of inhibitory interneurons during epileptiform activity. *J Neurosci*. 2014;34:3364-3377.
86. Kamali G, Smith RJ, Hays M, *et al*. Localizing the seizure onset zone from single pulse electrical stimulation responses using transfer function models. *Annu Int Conf IEEE Eng Med Biol Soc*. 2020;Jul:2524–22527.
87. Yan Q, Gaspard N, Zaveri HP, *et al*. The connectivity index: An effective metric for grading epileptogenicity. *J Neurosurg*. 2020; 133:971–9978.
88. Jiang H, Kokkinos V, Ye S, *et al*. Interictal SEEG resting-state connectivity localizes the seizure onset zone and predicts seizure outcome. *Adv Sci*. 2022;9:e2200887.
89. Malladi R, Kalamangalam G, Tandon N, Aazhang B. Identifying seizure onset zone from the causal connectivity inferred using directed information. *EEE J Sel Top Signal Process*. 2016;10: 1267-1283.
90. Itzkovitz S, Alon U. Subgraphs and network motifs in geometric networks. *Phys Rev E*. 2005;71:026117:1-9.
91. Tempel T, Frings C, Pastötter B. EEG beta power increase indicates inhibition in motor memory. *Int J Psychophysiol*. 2020; 150:92-99.
92. Hammond C, Bergman H, Brown P. Pathological synchronization in Parkinson's disease: Networks, models and treatments. *Trends Neurosci*. 2007;30:357-364.
93. Enatsu R, Piao Z, O'Connor T, *et al*. Cortical excitability varies upon ictal onset patterns in neocortical epilepsy: A cortico-cortical evoked potential study. *Clin Neurophysiol*. 2012;123:252-260.
94. Fingelkurts AA, Fingelkurts AA. Short-term EEG spectral pattern as a single event in EEG phenomenology. *Open Neuroimag J*. 2010;4:130-156.
95. von Stein A, Sarnthein J. Different frequencies for different scales of cortical integration: From local gamma to long range alpha/theta synchronization. *Int J Psychophysiol*. 2000;38:301-313.
96. Goyal A, Miller J, Qasim SE, *et al*. Functionally distinct high and low theta oscillations in the human hippocampus. *Nat Commun*. 2020;11:2469.
97. Whittington MA, Traub RD, Kopell N, Ermentrout B, Buhl EH. Inhibition-based rhythms: Experimental and mathematical observations on network dynamics. *Int J Psychophysiol*. 2000; 38:315-336.
98. Bartos M, Vida I, Jonas P. Synaptic mechanisms of synchronized gamma oscillations in inhibitory interneuron networks. *Nat Rev Neurosci*. 2007;8:45-56.
99. Sohal VS, Zhang F, Yizhar O, Deisseroth K. Parvalbumin neurons and gamma rhythms enhance cortical circuit performance. *Nature*. 2009;459:698-702.
100. Hermes D, Kasteleijn-Nolst Trenité DGA, Winawer J. Gamma oscillations and photosensitive epilepsy. *Curr Biol*. 2017;27: R336-R338.
101. Jiruska P, Alvarado-Rojas C, Schevon CA, *et al*. Update on the mechanisms and roles of high-frequency oscillations in seizures and epileptic disorders. *Epilepsia*. 2017;58: 1330-1339.
102. Paredes-Aragon E, AlKhaldi NA, Ballesteros-Herrera D, Mirsattari SM. Stereo-Encephalographic presurgical evaluation of temporal lobe epilepsy: An evolving science. *Front Neurol*. 2022;13:1–18.
103. Gotman J. Not just where, but how does a seizure start? *Epilepsy Currents*. 2019;19:229-230.
104. Buzsáki G, Wang X-J. Mechanisms of gamma oscillations. *Annu Rev Neurosci*. 2012;35:203-225.
105. Lundstrom BN, Gompel JV, Khadjevand F, Worrell G, Stead M. Chronic subthreshold cortical stimulation and stimulation-related EEG biomarkers for focal epilepsy. *Brain Commun*. 2019;1:fcz010.
106. Zamani Esfahlani F, Faskowitz J, Slack J, Mišić B, Betzel RF. Local structure-function relationships in human brain networks across the lifespan. *Nat Commun*. 2022;13:2053.
107. Shah P, Ashourvan A, Mikhail F, *et al*. Characterizing the role of the structural connectome in seizure dynamics. *Brain*. 2019; 142:1955-1972.
108. Myers JC, Smith EH, Leszczynski M, *et al*. The spatial reach of neuronal coherence and spike-field coupling across the human neocortex. *J Neurosci*. 2022;42:6285-6294.
109. Betzel RF, Bassett DS. Specificity and robustness of long-distance connections in weighted, interareal connectomes. *Proc Natl Acad Sci USA*. 2018;115:E4880-E4889.
110. Thivard L, Adam C, Hasboun D, *et al*. Interictal diffusion MRI in partial epilepsies explored with intracerebral electrodes. *Brain*. 2006;129:375-385.
111. Besson P, Bandt SK, Proix T, *et al*. Anatomic consistencies across epilepsies: A stereotactic-EEG informed high-resolution structural connectivity study. *Brain*. 2017;140: 2639-2652.
112. Donos C, Maliia MD, Mindruta I, *et al*. A connectomics approach combining structural and effective connectivity assessed by intracranial electrical stimulation. *Neuroimage*. 2016;132:344-358.
113. Kini LG, Bernabei JM, Mikhail F, *et al*. Virtual resection predicts surgical outcome for drug-resistant epilepsy. *Brain*. 2019;142: 3892-3905.
114. Olmi S, Petkoski S, Guye M, Bartolomei F, Jirsa V. Controlling seizure propagation in large-scale brain networks. *PLoS Comput Biol*. 2019;15:e1006805.
115. Proix T, Bartolomei F, Guye M, Jirsa VK. Individual brain structure and modelling predict seizure propagation. *Brain*. 2017; 140:641-654.
116. Gleichgerrcht E, Greenblatt AS, Kellermann TS, *et al*. Patterns of seizure spread in temporal lobe epilepsy are associated with distinct white matter tracts. *Epilepsy Res*. 2021;171: 106571.

117. Baum GL, Cui Z, Roalf DR, *et al*. Development of structure-function coupling in human brain networks during youth. *Proc Natl Acad Sci U S A*. 2020;117:771-778.
118. Conrad EC, Bernabei JM, Kini LG, *et al*. *How sensitive is functional connectivity to electrode resampling on intracranial EEG? Implications for personalized network models in drug-resistant epilepsy*. Cold Spring Harbor Laboratory; 2019.
119. Conrad EC, Bernabei JM, Kini LG, *et al*. The sensitivity of network statistics to incomplete electrode sampling on intracranial EEG. *Network Neuroscience*. 2020;4:484–4506.
120. Betzel RF, Medaglia JD, Kahn AE, Soffer J, Schonhaut DR, Bassett DS. Structural, geometric and genetic factors predict interregional brain connectivity patterns probed by electrocorticography. *Nat Biomed Eng*. 2019;3:902-916.